published by Ural Federal University
eISSN 2411-1414
chimicatechnoacta.ru

REVIEW
2024, vol. 11(2), No. 202411202
DOI: 10.15826/chimtech.2024.11.2.02

A review on agrowaste based activated carbons for pollutant removal in wastewater systems

Karinate Valentine Okiy [a] *, Joseph Tagbo Nwabanne [a], Walter Peter Echeng [b]

a: Department of Chemical Engineering, Nnamdi Azikiwe University, P.M.B. 5025, Awka 420218, Nigeria
b: Department of Chemical Engineering, Federal Polytechnic, Nekede 420218, Owerri, Nigeria
* Corresponding author: karinateokiy@gmail.com

This paper belongs to a Regular Issue.

Abstract

Environmental pollution from chemicals utilized in manufacturing, pharmaceuticals, and chemical process industries is of serious concern nowadays due to the contamination that ensues when these chemicals are discharged into water bodies. Activated carbon adsorption provides an efficient and economically viable means for mitigation of toxic chemicals (i.e., heavy metals, dyes, pharmaceutics, and antibiotics). However, the exorbitant cost of commercial activated carbons has resulted in the search for low-cost alternatives for the treatment of contaminated effluents. An exhaustive literature survey in this area is necessary to know the extent of work done in this area and seek out the gaps that future research will provide answers to. In this review, various works on activated carbon utilization, batch adsorption, fixed-bed adsorption (experimental and numerical studies) are summarized. This review elucidates the different kinetic and isotherm models of agrowastes-derived activated carbon materials in context with pollutants (dyes, heavy metals, pharmaceuticals, miscellaneous adsorbates) removal through batch and column methods. In addition, fixed-bed column adsorption/regeneration methods using various activated carbons derived from agrowastes are discussed. Among these methods, heavy metal adsorption from aqueous solutions by the activated carbons is the most efficient. The deployment of mathematical and machine learning approaches (ANN and novel GMDH algorithms) in optimization of batch and continuous adsorption processes are also highlighted. Numerical simulation of fixed-column adsorption systems for more improved industrial-scale column designs is described. Conclusions and future challenges of chemicals removal from polluted wastewater utilizing agrowaste-derived activated carbons are also presented.

Keywords

agrowastes-derived activated carbons
isotherm models
adsorption kinetics
batch
fixed-column adsorption

Received: 25.02.24
Revised: 08.03.24
Accepted: 14.03.24
Available online: 04.04.24

Key findings

- Numerical modeling and simulation provide faster, inexpensive means of assessing the quality of alternative activated carbons for wastewater treatment applications.
- Fixed-Bed adsorption column studies for wastewater treatment are still in its nascent stages, thus more research studies are required.
- Soft computing techniques such as ANN and particularly GMDH have seldom been applied to evaluate activated carbon adsorption performance in batch/fixed-bed adsorption systems. This application of these computational methods can significantly improve the design and optimization of activated carbon adsorptive separation processes.

1. Introduction

Adsorption refers to the process of extracting adsorbates (such as atoms, ions, and molecules) from gaseous and liquid solutions by retaining them on the surface of a solid substrate. In this adsorption process, the performance is influenced by fluid-solid equilibria and adsorption rates [1]. Adsorption can occur through both batch and fixed-column methods. Batch adsorption is commonly employed to separate pollutants from fluid media, especially when only small amounts of solute (adsorbate) are present in the solution. In a batch system, the concentration of adsorbate in contact with a specific quantity of adsorbent gradually diminishes as the adsorption process continues, ultimately reducing the adsorbent's efficacy for sorbate removal (Figure 1) [1, 2]. Batch adsorption studies are essential for assessing solute adsorption capacity, kinetic constants (k_2), and diffusive parameters ($D_{i,e}$) of the adsorbent(s). Mass transfer and adsorption properties are typically determined through batch experiments. However, in real-life water treatment/purification systems, operational constraints occur due to hydrodynamic effects (axial dispersion), channeling and non-equilibrium conditions.

The fixed-bed adsorber is a commonly used system in industrial applications for solute adsorption [2] for performing operations such as adsorption and desorption, effectively separating gaseous and liquid pollutants from fluid media. This system consists of a vertical cylindrical tube filled with adsorbent materials, typically activated carbon. The bed height ranges from 3 to 12 cm and is supported by materials such as glass wool, perforated plates, or screens (Figure 2) [1, 4]. Fixed-bed adsorbers are commonly operated in either downflow or upflow mode, with downflow being the preferred choice. However, upflow at high feed rates can result in attrition, fines loss, and particle fluidization [5].

In downflow mode, contaminated fluid (liquid or gas) enters the fixed-bed column from the top and interacts with the adsorbent particles. During this process, adsorbed molecules move through diffusion, convection, and dispersion from the bulk fluid into the adsorbent particle. As the adsorbate molecules come into contact with the adsorbent, intra-pellet diffusion and surface diffusion take place, resulting in the accumulation of sorbate molecules on the adsorbent material [7].

Solute adsorption in a fixed-bed column operating in downflow mode is influenced by several factors, including equilibrium conditions between the surrounding fluid and the adsorbent, mass transfer rates to the adsorbent particles, flowrates, and intra-particle diffusion. The adsorption process within the fixed-bed adsorber is characterized by unsteady state behavior and dynamics. Specifically, it can be divided into three distinct zones: the clean zone, the mass transfer zone, and the saturated zone. The clean zone marks the initiation of solute molecule adsorption, while the mass transfer zone is where non-equilibrium adsorption of the adsorbate occurs. Finally, in the saturated zone, the adsorbent reaches its maximum capacity, and no further adsorption takes place [8–10]. The height of the mass transfer zone within the adsorber that significantly influences the concentration changes is related to fluid velocity. In addition, the usable bed capacity, determined by the time at which the effluent concentration reaches the maximum permissible level (exhaustion time), plays a crucial role in the design of fixed-bed adsorbers [1, 2, 11]. For adsorption-based separation applications, activated carbon stands out as the preferred adsorbent due to its remarkable effectiveness, surface reactivity, thermal stability and versatility in separating various pollutants, including dyes, pharmaceuticals, heavy metals, and antibiotics, commonly found in wastewater [12, 13].

Activated carbon adsorption offers an efficient and economically viable solution for reducing polluted effluent [14]. However, industrial activated carbons derived from natural sources like wood, coal, and peat are costly and not readily available in-situ. The high expenses associated with commercial activated carbons have prompted the exploration of low-cost alternatives, including agricultural wastes [15]. Unmodified agricultural wastes (biomass), when used as alternative adsorbents, demonstrate partial to moderate adsorption capacities, rendering them ineffective for treating polluted wastewater.

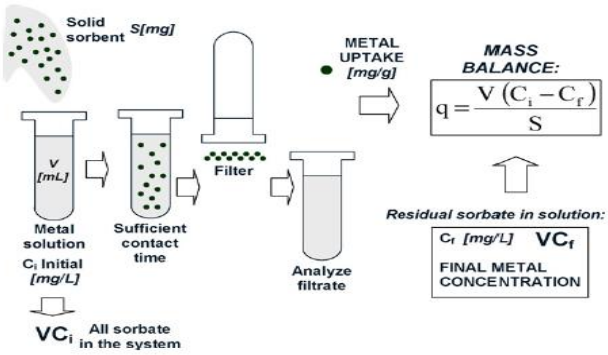

Figure 1 Batch adsorption set-up for removal of contaminants from aqueous solutions [3].

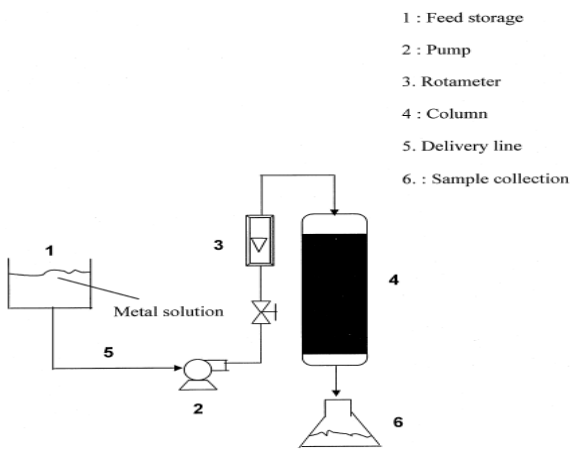

Figure 2 Schematic of experimental setup for adsorption in the fixed-column [6].

 DOI: 10.15826/chimtech.2024.11.2.02

However, modifying agricultural wastes through physical methods (such as thermal activation) or with chemical reagents (like chemical activation) enhances their adsorption capacity by creating a well-organized crystalline structure and improving pore texture in the resulting solid carbon [16, 17].

In this review, we will delve into the mechanisms of adsorption, isotherm, and kinetic models. These models are applicable for assessing the quality of produced activated carbons. Furthermore, we will explore various works related to adsorptive separation of dyes, heavy metals, pharmaceuticals, and other miscellaneous sorbates from polluted effluents. Furthermore, we will review fixed-bed adsorption through both experimental and numerical approaches. Lastly, we will identify research gaps and propose new directions for future research work.

2. Mechanism of adsorption

Activated carbon adsorption typically involves a four-step process: transport of solute through the adjoining liquid film to the external surface of the adsorbents (film diffusion), bulk transfer of diffusing molecules (solute) within the adsorbent particle (intra-particle pore diffusion), migration of the solute on the surface-active sites within the micropores of the activated carbons (intra-particle surface diffusion), and adsorption/desorption at surface active sites on the adsorbent surface (surface reaction phenomenon) [18].

In the aqueous (water) adsorption process, three main interactions affect the adsorption of sorbate molecules by activated carbon: 1) adsorbate-water (solvation effect); 2) adsorbate-activated carbon (hydrogen bonding, π–π interactions, surface complexation, ion exchange, electrostatic interactions, precipitation), and 3) activated carbon-water (Figure 3) [19].

2.1. Adsorbate-water interactions

The physico-chemical properties (molecular weight, solubility, PK_a, molar volume, surface area etc.) of the adsorbate can impact the interactions between the molecules and water solvent. The hydrophilic (water-loving) nature of metallic adsorbates ions (cations) can result in interaction of the partial charges of the cations with partial charges on the water solvent. The negative poles of the water solvent (hydroxyl ions) surround the positive pole of the adsorbate ions. Clustering of the hydroxyl ions (OH^-) around the adsorbate molecules results in dissolution of the solute (adsorbate). Hence, the much stronger adsorbate-water molecular interactions relative to those of water-water or adsorbate-adsorbate molecules will lead to reduced adsorption. On the other hand, a hydrophilic adsorbate (organic compound) will outflow from the aqueous solution and adhere to the surface of activated carbon, which also has little affinity for water (enhanced adsorption). This behavior is known as solvent-motivated adsorption [21].

2.2. Adsorbate-activated carbon interactions

The porous structure (BET surface area, pore size distribution, and pore volume) and chemical surface (surface chemistry) significantly influence the adsorption equilibria and kinetics for each specific adsorbate (pollutant). A large surface area composed of a huge number of carbon atoms (sorption sites) is necessary for retention of the adsorbate molecules on the activated carbon. The micropores constitute most of the specific surface area of the activated carbon. Hence, the size of the adsorbate molecules adsorbed must be slightly smaller than the size of these smaller pores to allow them to reach the internal adsorption surface of the porous carbon. Thus, pore size distribution is an important property for characterizing the absorption capacity of activated carbon. The surface chemistry (acidity, aromatic degree, and polarity) of the activated carbon as well as the solution chemistry can retard or augment adsorption. Oxygen is major non-carbon element present in the functional groups on the pore walls of the activated carbon. These surface functional groups augment the polarity of the carbon surface and promote different adsorbate-activated carbon interactions (chemical adsorption reactions) unique to the activated carbon [19]. Hence, the reactivity of each individual activated carbon is more or less dependent on its characteristic surface functional groups.

The interactions that can occur between adsorbate and activated carbon include hydrogen bonding, electrostatic interactions, π–π interactions, precipitation, ion exchange, and surface complexation.

2.2.1. Hydrogen bonding

Hydrogen bonding is a physical adsorption mechanism, which can be attributed to the large partial positive charge (σ^+) on hydrogen (acceptor) atom covalently bonded to the oxygen and/or nitrogen atoms present in the adsorbate molecule. The H-bond polar interactions with adsorbate (pollutants) favours the adsorption process due to the formation of hydrogen (coordinate) bonds between the amine (N–H) or hydroxyl (OH^-) groups in the activated carbon and the heavy metal (adsorbate) acceptor ions in solution.

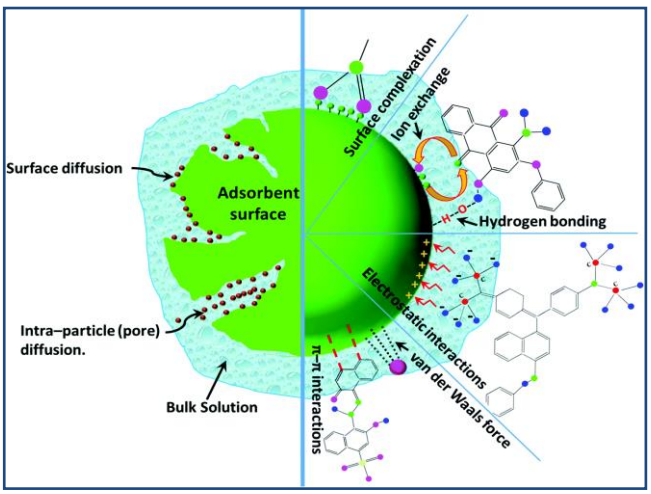

Figure 3 Mechanisms of adsorption in activated carbons [20].

 DOI: 10.15826/chimtech.2024.11.2.02

2.2.2. Electrostatic interactions

Electrostatic interaction is a major mechanism for the adhesion of adsorbate molecules onto activated carbon. Mostly, activated carbons are amphoteric in nature, with variable surface charges dependent on surface charge density and solution chemistry. The ionic environment of the solution (solution pH) affects the speciation of adsorbate molecules in solution and surface charge of activated carbon (AC's). If the solution pH is greater than the pH zero-point charge (zero surface charge density) of the activated carbon, the surface acidic/basic functional groups are deprotonated and become predominantly negatively charged. Consequently, electrostatic attraction occurs between the adsorbate molecules (metallic cations) and negatively charged adsorption sites on the activated carbon's (AC's) surface. Electrostatic attraction ensues between the adsorbate molecule and activated carbon surface when the surface charges are dissimilar (opposite). In the process, the Gibbs free energy of adsorption decreases, favoring adsorption reaction (higher adsorption capacity). Electrostatic attraction can also be a secondary mechanism for the sorption of adsorbate molecules by activated carbon, occurring in conjunction with other mechanisms such as surface complexation, ion exchange, and precipitation (cooperative mechanism).

2.2.3. π–π interactions

π–π interactions are mainly attributed to interactions between the graphitic (aromatic ring) π-electrons of activated carbon and the electron-donating (positively charged) adsorbate molecules. π–π interactions are also known as π–π electron donor-acceptor (EDA) interactions. Notably, π–π interactions (non-covalent) involving the π system are attenuated by the presence of nitrogen and oxygen containing surface functional (electron-withdrawing) groups, resulting in a significant drop in the π electron density of individual grapheme (aromatic) layers within the carbon matrix. π–π interactions are analogous to electrostatic attractions.

2.2.4. Precipitation

The precipitation mechanism involves the formation of chemical precipitates (solid products), either on a solid phase (activated carbon) or in solution. Precipitation is a major mechanism for heavy metals removal by activated carbons, which occurs synchronously with other mechanisms such as electrostatic interactions, surface complexation, and ion exchange during adsorption. In the process, heavy metals are separated from solution as solid pigments, minerals, crystals, etc. The precipitation of adsorbates (contaminants) from aqueous solutions, can promote adsorbate mass transport (diffusion), possibly enhancing adsorption kinetics comparative to other adsorption mechanisms.

2.2.5. Ion exchange

The ion exchange mechanism involves ion exchange via chemical reactions between adsorbate molecules (metallic cations) in solution and protons on oxygen containing functional groups in the solid phase (activated carbon). In the process, electroneutrality must be maintained. The ion exchange efficiency for heavy metals adsorption by activated carbons is largely dependent on the molecular area of the adsorbate molecule (metallic cation) and surface chemistry of the activated carbon. The ion exchange process can be represented as follows:

$$Pb^{2+}_{(solution)} + -COOH_{(solid\ carbon)} \rightleftharpoons -COOPb^{+}_{(solid\ carbon)} + H^{+}_{(solution)} \quad (1)$$

Positively charged adsorbate (Pb^{2+}) in solution diffuse into the pores of the activated carbon and exchange with the H^+ in the carboxyl surface groups present in activated carbon. The solution pH is a key parameter affecting the ion exchange process. At low (acidic) pH, ion exchange is more likely the predominant mechanism due to increased number of protons (H^+) available to saturate the adsorbate (metal)-binding sites. Further, the ionic environment of the solution (solution pH) is altered after H^+ is released from metal-occupied sorption sites on activated carbon surface during the adsorption.

2.2.6. Surface complexation

Surface complexation involves the interaction of metallic adsorbate ions with carboxylic and other weakly acidic functional groups in activated carbons to form multi-atom structures (e.g., surface complexes). The surface complexation process can be represented as follows:

$$\equiv C\text{–}OH + Pb^{2+} \leftrightarrow C\text{–}OPb^{+} + H^{+}\ (\text{Monodentate complexes}) \quad (2)$$

$$\equiv C\text{–}OH \quad \equiv C\text{–}OH \quad \searrow$$
$$+\ 2Pb^{2+} \leftrightarrow \qquad Pb + 2H^{+} \quad (3)$$
$$\equiv C\text{–}OH \quad \equiv C\text{–}OH \quad \nearrow$$
$$(\text{Bidentate complexes})$$

The oxygen containing functional (phenol) groups on the activated carbon's (AC's) surface bind with Pb^{2+} ions to form surface complexes. The p_{Ka} values of the phenolic groups play an essential role in explicating the surface charge on the AC's surface. The p_{Ka} value is equal to the pH of a semi (partial) dissociated acid surface functional group (complex). When, the solution pH is higher than the p_{Ka} of the surface functional groups, the phenol groups dissociate and become predominantly negatively charged. The metallic sorbate ions can then be effectually bound to the negatively charged phenol groups in activated carbon by complexation. Surface complex formation (-inner and -outer sphere) is one of the principal mechanisms for the adsorption of heavy metals onto activated carbons. During surface complexation, adsorption is more favourable, when Gibb's free energy of adsorption is more negative. Hence, a similarly negatively charged adsorbate (co-ion) tends to be rejected (thermodynamically unfavourable), whilst an

 DOI: 10.15826/chimtech.2024.11.2.02

oppositely charged adsorbate (counter-ion) tends to be adsorbed onto the activated carbon surface (thermodynamically favorable) [18, 19, 21].

2.3. Activated carbon-water interactions

The surface charge (polarity) of activated carbon is variable, dependent on the different surface functional groups present. This is evident on immersion of activated carbon in aqueous solution, where the surface functional groups undergo dissociation, and, consequently, modify the polarity of the carbonaceous adsorbent. Likewise, oxygen and nitrogen containing (polar) groups can act as nucleation sites for accumulation of water molecules (micro-clusters) on the oxygen and nitrogen centers in the carbon surface (hydrogen bond formation) and, subsequently, the continuing stages of cluster formation and pore-filling. This interaction of basic, acid and neutral surface functional groups with water molecules increases the affinity of the activated carbon with water (hydrophilicity) and blocks the various pore openings. Thereby reducing the number of vacant sorption sites and restricting accessibility to adsorbate molecules for adsorption [21, 22, 23].

Distinguishing the predominant phenomena occurring in a distinctive adsorption system will provide insights into adsorption behavior and identify rate-determining step(s) to modify and improve the process rate.

3. Batch adsorption kinetic models

Adsorption kinetics plays a crucial role in determining the adsorbate uptake, which directly influences the residence time. In batch adsorption, the solute concentration reaches a steady state over time [24, 25]. According to Zhu et al. [26], 'Kinetic analysis is a fundamental aspect of understanding the rate of adsorption onto the adsorbent and the underlying adsorption mechanism.' Adsorption kinetic studies involve employing models to represent the adsorption process and determine the kinetics of sorption. These mathematical models are typically categorized as adsorption diffusion models and adsorption reaction models. Their purpose is to provide useful information for evaluating the performance of adsorbents [24]. The adsorption diffusion model involves a three-step process: the transport of solute through the liquid film surrounding the adsorbent to reach its external surface (known as film diffusion), the bulk transfer of diffusing molecules (solute) within the adsorbent particle (referred to as intra-particle diffusion), and finally, adsorption/desorption occurring at the surface-active sites during the liquid/solid adsorption process [17, 18]. The adsorption diffusion model was developed under the premise that mass action plays a negligible role in determining the overall rate of the adsorption process. Instead, the overall rate is governed by film diffusion and/or intra-particle diffusion processes, which operate differently from the rapid mass action (surface reaction) step. Consequently, in the study of adsorption kinetics, researchers often focus on the intra-particle diffusion and film diffusion steps, while overlooking the mass action step. Notable adsorption diffusion models used for determining kinetics include Boyd's model (Eq. 2.5), the Weber-Morris model (Eq. 2.8), and the Homogeneous Solid Diffusion model (Eq. 2.9) [28, 29].

3.1. Boyd model

Boyd et al. introduced an intra-particle diffusion model to analyze adsorption kinetics [30]. The Boyd model is characterized by the following kinetic expressions [31, 32]:

$$F = 1 - \left({}^{6}/_{\Pi^2}\right)\sum_{N-1}^{\alpha} {}^{1}/_{n^2} \exp(-n^2 B \cdot t), \tag{4}$$

where B is the time constant,

$$B = \frac{\pi^2 D_i}{R^2}. \tag{5}$$

Simplifying Equation 4 by applying Fourier transform and integrating, we obtain the following linear approximation for $F = {}^{q_t}/_{q_e} < 0.85$ [33]:

$$B \cdot t = \left(\sqrt{\pi} - \sqrt{\pi - \left(\pi^2 \cdot {}^{F}/_{3}\right)}\right)^2, \tag{6}$$

where $F = {}^{q_t}/_{q_e}$ is the function of solute adsorbed at different times, $B \cdot t$ is a mathematical function of F, n is the Freundlich isotherm constant of the adsorbate, q_e is the amount of metal ions adsorbed at equilibrium (mg·g^{-1}), B is the Boyd number(-), D_i is the effective intra-particle diffusion coefficient $\left(\frac{m^2}{s}\right)$, q_t amount of metal ion adsorbed at any given time t (mg·g^{-1}) and R is the radius of the adsorbent particle (m).

The Boyd model has been effectively utilized for kinetic modeling of diverse adsorption systems, including the adsorption of phenol using a polymeric adsorbent (NDA-100) under varying conditions of temperature and initial concentration [34, 35].

3.2. Weber-Morris model

Weber-Morris introduced an intra-particle diffusion model to analyze adsorption kinetics. This model is based on the observation that, in most adsorption processes, the rate of solute removal (or solute uptake) is nearly proportional to the square root of the contact time $\left(t^{1/2}\right)$ [34, 36, 37].

$$q_t = k_{id} t^{1/2} + C_i, \tag{7}$$

where, $t^{1/2}$ is the square root of time, q_t is the amount of metal ions adsorbed at any given time t, k_{id} is the intra-particle diffusion rate constant $\left(\text{mg/g min}^{1/2}\right)$ and C_i is the thickness of the boundary layer(mg/g).

3.3. Homogeneous solid diffusion model

Matthews and Weber [38] proposed an intra-particle diffusion model suitable for evaluating mass transfer in a homogeneous and amorphous sphere. The homogeneous solid

 DOI: 10.15826/chimtech.2024.11.2.02

diffusion model (HSDM) is described by the equations below [26, 39]:

$$\frac{\partial q}{\partial t} = \frac{D_s}{r^2}\frac{\partial}{\partial r}\left(r^2\frac{\partial q}{\partial r}\right). \quad (8)$$

Overall mass balance

$$\frac{dC_b}{dt}V = -M\frac{d\bar{q}}{dt}. \quad (9)$$

Solid phase mass balance

$$\bar{q} = \frac{3}{(R)^3}\int_0^R q\,(r,t)r^2 dr. \quad (10a)$$

Initial condition

$$(q(r,0) = 0). \quad (10b)$$

Boundary conditions

$$(\frac{\partial q}{\partial r} = 0 \text{ for } r = 0); \quad (10c)$$

$$\rho_p D_s\frac{\partial q}{\partial r} = k_f(C_b - C_s), (r = R); \quad (11)$$

$$q_s = K_F C_s^n, (r = R), \quad (12)$$

where D_s is the intra-particle diffusion coefficient (m^2/s), q is the average solid phase concentration in equilibrium with liquid phase concentration at solid-liquid interface (mg/g), r is the radial coordinate (m), t is time (min), C_b is the bulk liquid phase concentration (mg/m^3), V is the liquid phase volume (m^3), $\bar{q}$ is the average adsorbed phase concentration (mg/g), M is the total mass of carbon (g), R is the radius of adsorbent particle (m), $q(r,t)$ is the adsorbed phase concentration (mg/g), ρ_p is the apparent density of particle (g/m^3), k_f is the external mass transfer coefficient (m/s), C_s is the liquid phase concentration at the solid-liquid interface (mg/m^3), q_s is the adsorbed phase concentration at solid-liquid interface (mg/g), K_f is the Freundlich isotherm capacity constant (μg/mg) and n is the Freundlich isotherm constant.

Kwon [40] utilized the orthogonal collocation method to transform the previously mentioned partial differential equations (PDEs) into a system of ordinary differential equations (ODEs). Subsequently, Laplace transforms are employed to convert these ODEs into algebraic equations. Solving these algebraic equations yields the adsorbed phase concentration denoted as $q(r,t)$. Finally, this solution is substituted into Equation 7 [39, 41]:

$$\frac{\bar{q}}{q_0} = 1 - \frac{6}{\pi^2}\sum_{n=1}^{\infty}\frac{1}{n^2}\exp\left(\frac{-D_s n^2\pi^2 t}{R^2}\right). \quad (13)$$

Simplifying Equation 13, we obtain the following linear forms.

For a short residence time ($\bar{q}/q_\infty < 0.3$),

$$\frac{\bar{q}}{q_\infty} = 6\left(\frac{D_s}{R^2\pi}\right)^{1/2}t^{1/2}. \quad (14)$$

For a long residence time ($\bar{q}/q_\infty > 0.3$),

$$\ln\left(1 - \frac{\bar{q}}{q_\infty}\right) = \frac{-D_s\pi^2}{R^2}t + \ln\frac{6}{\pi^2}. \quad (15)$$

The HSDM has demonstrated successful application in kinetic studies for diverse adsorption systems. Examples include the adsorption of pentachlorophenol using activated carbon and the adsorption of salicylic acid using hypercross-linked polymeric adsorbent (NDA-99) [39].

Similarly, adsorption reaction models have been widely employed to elucidate adsorption kinetics. Unlike adsorption diffusion models, these models do not account for the specific mechanisms underlying the adsorption process [24, 42].

Instead, adsorption reaction models are utilized under the premise that the overall adsorption rate primarily depends on the sorbate's rate of adsorption onto active sites at the adsorption front (a surface reaction phenomenon) [24]. Notable adsorption reaction models include the pseudo-first-order kinetic model, pseudo-second-order kinetic model, and the Elovich kinetic model [43, 44].

3.4. Pseudo first order kinetic model

Lagergren proposed a first-order rate equation to describe the kinetics of adsorption for malonic acid and oxalic acid onto charcoal. This model takes the form [39, 45]:

$$\frac{dq_t}{dt} = k_1(q_e - q_t). \quad (16)$$

Boundary conditions

$$q = 0 \text{ at time} = 0, \quad (17)$$

where, q_t is the amount of metal ions adsorbed ($mg\cdot g^{-1}$) at any given time t (min), q_e is the amount of metal ions adsorbed at equilibrium ($mg\cdot g^{-1}$) and k_1 is the pseudo first order rate constant for the adsorption process (min^{-1}).

Integrating Equation 16, applying the stated boundary conditions gives:

$$\log(q_e - q_t) = \log q_e - \frac{k_1}{2.303}t. \quad (18)$$

Rearranging Equation 18, we obtain the non-linearized form:

$$q_t = q_e - q_e\exp(-k_1 t). \quad (19)$$

The first-order rate equation proposed by Lagergren for adsorption process kinetics (related to adsorption capacity) is commonly known as the pseudo first-order rate equation. This distinction is necessary to differentiate it from the well-established kinetic equations correlated with the concentration of adsorbate in solution (associated with chemical reactions) [39, 45].

Recently, researchers have extensively applied this model in kinetic studies for various adsorption systems. These systems include the removal of malachite green using

 DOI: 10.15826/chimtech.2024.11.2.02

oil palm trunk fiber, lead adsorption from aqueous solutions using peat moss, and methylene blue adsorption using broad bean peels [39, 46–48].

3.5. Pseudo second order kinetic model

Ho et al. [49] developed a pseudo-second-order rate equation to investigate the adsorption of bivalent metal ions onto peat adsorbent. This chemisorption kinetics model is expressed as follows [50]:

$$\frac{dq_t}{dt} = k_2(q_e - q_t)^2, \quad (20)$$

where q_t is the amount of metal ions adsorbed (mg/g) at any given time t (min), q_e is the amount of metal ions adsorbed at equilibrium (mg/g) and k_2 is the pseudo-second-order rate constant for the adsorption process (g·mg^{-1}·min^{-1}).

Rearranging Equation 20, we obtain the kinetic expression:

$$\frac{dq_t}{(q_e - q_t)^2} = k_2 dt. \quad (21)$$

Boundary conditions

$$q = 0 \text{ at time} = 0. \quad (22)$$

Integrating Equation 21 applying the stated boundary conditions, then rearranging gives:

$$\frac{t}{q_t} = \frac{1}{q_e^2 k_2} + \frac{t}{q_e}. \quad (23)$$

Ho's second-order rate equation is commonly known as the pseudo-second-order rate equation, distinguishing it from the kinetic equations that rely on solution concentration. This model postulates that the rate-determining step is the surface reaction phenomenon (mass action) [32, 50, 51].

Recently, researchers have effectively employed the pseudo-second-order rate equation in kinetic studies across diverse adsorption systems. These systems include the adsorption of dyes, metal ions, organic substances, oils, and herbicides from aqueous solutions, utilizing various adsorbents like peat, tamarind fruit shell, and oil palm trunk fiber [39, 52, 53].

3.6. Elovich kinetic model

Zeldowitch [54] proposed a chemisorption kinetic model to describe the rate of carbon monoxide adsorption onto solid manganese dioxide. This kinetic equation, also referred to as the Roginski-Zeldovich equation, is expressed as follows [55]:

$$\frac{dq_t}{dt} = \beta e^{-\alpha q}. \quad (24)$$

Boundary conditions

$$q = 0 \text{ at time} = 0. \quad (25)$$

Integrating Equation 24 applying the stated boundary conditions gives, after rearranging:

For $\alpha\beta t >> 1$,

$$q_t = \frac{1}{\beta}\ln \alpha\beta + \frac{1}{\beta}\ln t, \quad (26)$$

where q_t is the amount of adsorbate (mg·g^{-1}) adsorbed at any given time t (min), α is the initial adsorption rate (mg·g^{-1}·min^{-1}) and β is the desorption constant (g·mg^{-1}).

The Elovich equation, widely employed for modeling gas/solid adsorption processes, has successfully described the kinetics of various adsorption systems. These include the adsorption of Cr (VI) ions by chitin, cadmium removal from effluents using bone char, and Cu (II) ions adsorption using chitosan [39, 56].

Common adsorption reaction models do not precisely capture the intricacies of the adsorption process. Consequently, they fail to provide sufficient insights into the associated adsorption (diffusion) mechanisms. In physical adsorption processes, the rates of adsorption and desorption within porous adsorbents are primarily governed by mass transfer within the pore network rather than kinetics related to adsorption on the adsorbent surface. For a more accurate representation of the adsorption process, utilization of adsorption diffusion model(s) is considered. These models can yield valuable information for designing fixed-bed systems, including parameters such as the surface diffusion coefficient (D_s) and the rate-controlling step [31, 57, 58].

4. Batch adsorption isotherm models

Adsorption isotherms describe the mathematical and experimental relationships between the equilibrium concentration of the adsorbate (solute) on the adsorbent (solid phase) and the concentration of the residual solute in the fluid phase at a fixed temperature [59, 60]. These isotherms can be represented by a general expression [61, 62]:

$$Q = \frac{V}{m}(Ca_o - C) + Qa_o. \quad (27)$$

For most adsorption systems, the initial solute concentration (Q_{aO}) is considered negligible. Thus, simplifying Equation 27 gives:

$$Q = \frac{V}{m}(Ca_o - C), \quad (28)$$

where Q is the amount of solute retained on the adsorbent (mg/g), Qa_O is the initial amount of solute retained on the adsorbent (mg·L^{-1}), V is the volume of the solution (L), m is the mass of adsorbent (g), Ca_O is the initial concentration of solute in solution (mg·L^{-1}) and C is the final concentration of solute in solution (mg·L^{-1}).

The adsorption isotherm provides insight into the distribution of adsorption potentials, which represent the intensity of attractive forces on the surface and within the pores of the adsorbent. These forces, including van der Waals (London dispersion) and chemical bond interactions, play a crucial role in the adsorption process [23]. The adsorption isotherm provides valuable insights into various aspects, including the equilibrium amounts of adsorbate molecules (representing adsorption capacity), the structure

 DOI: 10.15826/chimtech.2024.11.2.02

of porous networks, geometric arrangements, pore texture, surface functionalities, and the non-uniform distributions of adsorption potential (referred to as energetic heterogeneity) within the adsorbent material. Consequently, understanding the adsorption isotherm is crucial for optimizing the use of adsorbents and designing effective adsorption systems [63, 64].

The commonly used two-parameter equations for analyzing equilibrium isotherm data include Langmuir, Freundlich, Temkin, Dubinin-Radushkevich, and Harkins-Jura isotherm models [64–66].

4.1. Langmuir isotherm model

In 1916, Irving Langmuir introduced a semi-empirical isotherm model to investigate the adsorption of gases onto solid surfaces. The derived equation, based on presumed kinetic theory, establishes a relationship between the number of occupied adsorption sites on the adsorbent surface and the pressure at equilibrium for a fixed temperature. The Langmuir equation describes adsorption phenomena by assuming maximal uni-molecular (single-layer) adsorption onto a solid surface composed of a limited number of surface-active sites. These sites exhibit equivalent (uniform) adsorption potentials (energies) and highly localized interactions between the adsorbate and the adsorbent. Importantly, there is virtually no transmigration of adsorbate within the surface plane (no adsorbate-adsorbate interactions) [67, 68]. McCabe et al. [1] asserted that the Langmuir equation is suitable for adsorption systems characterized by weak interactions between gas (adsorbate) and solid (adsorbent). This relationship is expressed as follows [69]:

$$\mathrm{P/(X/m)} = 1/a + (a/b)\,P, \tag{29}$$

where P is the equilibrium pressure for a given amount of substance adsorbed (kg·m·s^{-1}), m is the amount of adsorbent (g), X is the amount substance adsorbed (mg), a and b are Langmuir constants.

Alternatively,

$$q_e = \frac{Q_0 b C_e}{1 + bC_e}. \tag{30}$$

The linearized form of Equation 27 is represented as [67]:

$$\frac{1}{q_e} = \frac{1}{Q_o} + \frac{1}{bQ_oC_e}, \tag{31}$$

where q_e is the amount of adsorbate per unit mass of adsorbent at equilibrium (mg/g), Q_o is the monolayer adsorption capacity of adsorbent for monolayer adsorption (mg·g^{-1}), b is Langmuir constant related to the net enthalpy or energy of adsorption (L·mg^{-1}) and C_e is the liquid phase concentration of adsorbate at equilibrium (mg·L^{-1}).

In their work, Hall et al. [70] introduced a dimensionless equilibrium parameter denoted as "R", which is also known as the separation factor. This parameter was employed to investigate the application of the Langmuir adsorption isotherm. The fundamental assumption underlying this study is the conformity of the adsorption process with the Langmuir model. Notably, the parameter "*R*" offers valuable insights into the characteristics of the adsorption isotherm. It serves as a tool to determine the favorability of the adsorption process (Table 1).

The separation factor R is defined as [67]:

$$R = \frac{1}{1 + bC_0}, \tag{32}$$

where C_o is the initial solute concentration (mg·L^{-1}).

4.2. Dual-site Langmuir isotherm model

The variations in adsorption energy across distinct sorbent surface sites are elucidated by modifying the Langmuir isotherm model. This particular model is constructed based on the assumption that the sorbent possesses two types of adsorption sites: strong (type 1) and weak (type 2) sorption sites [71, 72]. Experimental adsorption data for liquid-solid adsorption systems can be interpreted using the dual-site Langmuir isotherm model, as expressed in Equation 33:

$$q_e = \frac{Q_1 b_1 C_e}{1 + b_1 C_e} + \frac{Q_2 b_2 C_e}{1 + b_2 C_e}, \tag{33}$$

where Q_1 and Q_2 are the monolayer adsorption capacities of adsorption site 1 and 2 (mg·g^{-1}), b_1 and b_2 are the Langmuir constants for the respective adsorption site (L·mg^{-1}) and C_e is the liquid phase concentration of adsorbate in equilibrium (mg·L^{-1}) [72, 73].

4.3. Freundlich isotherm model

Freundlich [74] proposed an empirical relation to describe the adsorption of acetic acid onto charcoal. The equation establishes a connection between the amount of solute adsorbed per unit mass of adsorbent (specific adsorption) and the equilibrium concentration of adsorbate in solution at a constant temperature. The Freundlich equation sheds light on equilibrium behavior on inhomogeneous surfaces, considering non-uniform distribution of adsorption potentials (energetic heterogeneity) and infinite adsorptive capacity as the sorbate concentration approaches its saturation point [75, 76]. The Freundlich isotherm applies to reversible adsorption processes characterized by variations in adsorption energy associated with progressive multilayer formation (surface coverage). However, its applicability is limited in predicting adsorption behavior for gases at pressures exceeding the saturation pressure (P_s) [77, 78]. The Freundlich equation is empirically represented as [69]:

$$x/m = KC^{\mathrm{n}}, \tag{34}$$

Table 1 Values of separation factor R indicating nature of adsorption isotherm [67].

Value of *R*	Information about the adsorption
$R > 1$	Unfavourable
$R = 1$	Linear
$0 < R < 1$	Favourable
$R = 0$	Irreversible

 DOI: 10.15826/chimtech.2024.11.2.02

where m is the amount of adsorbent (g), x is the amount of substance adsorbed (mg), C is the equilibrium liquid phase concentration of adsorbate (mg), K and n are Freundlich constants related to amounts of adsorbate and adsorbent.

Alternatively,

$$q_e = K_F C_e^{1/n}. \quad (35)$$

The linearized form of Equation 35 is represented as [62, 67, 68, 79].

$$\log q_e = \log K_F + \left(\frac{1}{n}\right) \log C_e. \quad (36)$$

For the Freundlich isotherm, q_e is the amount of adsorbate adsorbed per unit mass of adsorbent (mg/g), K_F is the Freundlich capacity factor indicative of the relative adsorption capacity of the adsorbent $\left(\text{mg}^{1-1/n} L^{1/n} \text{g}\right)$, C_e is the concentration of adsorbate in solution at equilibrium (mg/L), while n (dimensionless) is the adsorption intensity parameter indicative of surface heterogeneity or magnitude of the adsorption driving force. For Freundlich exponent (n) values within the range of $0 < n < 10$, the adsorption isotherm displays a convex upward shape, analogous to favorable adsorption. However, for $n > 10$, the adsorption isotherm approaches a limiting case of favorable adsorption, which corresponds to irreversible adsorption [64, 80].

4.4. Temkin isotherm model

Temkin and Pyzhev [81] developed an isotherm equation based on experimental observations related to nitrogen (N_2) adsorption using iron catalysts (chemisorption mechanism). The equation relies on the assumption that the free energy (heat) associated with adsorption decreases linearly with surface coverage due to interactions between the adsorbent and adsorbate molecules [81, 82]. The Temkin isotherm equation provides insights into the occurrence of chemical adsorption mechanisms. This equation is expressed as [65, 83, 84]:

$$q_e = \frac{RT}{b_T} \ln A_T C_{eq}. \quad (37)$$

The linearized form of Equation 37 is represented as:

$$q_e = \frac{RT}{b_T} \ln A_T + \frac{RT}{b_T} \ln C_{eq}. \quad (38)$$

Substituting B for $\left(\frac{RT}{b_T}\right)$ in Equation 38 gives:

$$q_e = B \ln A_T + B \ln C_{eq}, \quad (39)$$

where q_e is the amount of adsorbate adsorbed per unit mass of adsorbent (mg·g^{-1}), A_T is the equilibrium binding constant indicative of maximum binding energy (L·g^{-1}), B (RT/b_T) is the Temkin isotherm constant related to heat of adsorption (dimensionless), b_T is the variation of adsorption energy (J/Mol), R is the universal gas constant (8.314 J/Mol·K), T is the absolute temperature (K) and C_{eq} is the concentration of adsorbate in solution at equilibrium (mg·L^{-1}).

4.5. Hakins-Jura isotherm model

Harkins and Jura [85] introduced an isotherm model to investigate the adsorption of solutes from both ideal and attenuated (dilute) solutions onto solid surfaces [85]. The Harkins-Jura isotherm equation was formulated to consider the impact of non-uniform (heterogeneous) pore distribution on multilayer adsorption onto the adsorbent. The Harkins-Jura correlation is expressed as follows [86, 87]:

$$q_e = \left(\frac{A}{B + \log C_e}\right)^{1/2}, \quad (40)$$

$$B = \frac{-qS^2}{4.606RTN}. \quad (41)$$

The linearized form of Equation 40 is represented as:

$$\frac{1}{q_e^2} = \frac{B}{A} + \left(\frac{1}{A}\right) \log C_e, \quad (42)$$

where q_e is the amount of adsorbate per unit mass of adsorbent at equilibrium (mg·g^{-1}), S is the specific surface area of the adsorbent (m^2.g^{-1}), q is a constant independent of the nature of adsorbent, T is the absolute temperature (K), N is the Avogadro number ($6.022 \cdot 10^{23}$), R is the universal gas constant (8.314 J/Mol·K), C_e is the liquid phase concentration of adsorbate at equilibrium (mg·L^{-1}) and A and B are isotherm constants.

The Harkins-Jura isotherm equation has found application in various fluid/solid adsorption systems. These include the adsorption of nitrogen using carbon black (Spheron 6), aniline adsorption from toluene using charcoal or titanium dioxide, and the adsorption of argon using nitrile. Additionally, it has been employed for the adsorption of alcohol vapors using charcoal [66, 86].

4.6. Dubinin-Radushkevich isotherm model

In 1947, Dubinin and Radushkevich proposed a semi-empirical relation to investigate the adsorption of benzene onto activated carbon. This isotherm equation has found extensive application in elucidating multilayer formation within microporous solids (adsorbents) characterized by energetically heterogeneous surfaces [88, 89]. The Dubinin-Raduskevich equation quantitatively describes adsorption data by plotting the logarithm of the adsorbed amount against the square of the potential energy. This relationship is known as the characteristic adsorption curve and is closely tied to the porous structure of the adsorbent [87, 90]. The Dubinin-Raduskevich isotherm equation describes multilayer adsorption on the adsorbent surface, based on the Polanyi potential theory of adsorption. This theory assumes that adsorptive-adsorbate interactions primarily arise from London-dispersion forces and the presence of surface-active sites with non-uniform adsorption energies (energetic heterogeneity) [88]. The Dubinin-Raduskevich equation is mathematically expressed as follows [87, 91]:

$$q_e = q_m e^{-\beta \varepsilon^2}, \quad (43)$$

 DOI: 10.15826/chimtech.2024.11.2.02

$$\varepsilon = RT\left(1 + \frac{1}{C_e}\right). \quad (44)$$

The linearized form of Equation 43 is represented as:

$$\ln q_e = \ln q_m - \beta\varepsilon^2, \quad (45)$$

where q_m is the theoretical saturation capacity of adsorbent(mg·g^{-1}), q_e is the amount of metal ions adsorbed at equilibrium (mg·g^{-1}), ε is the Polanyi potential indicative of the amount of energy required to extract an adsorbate molecule from its adsorption site to infinity in the solution (J^2·g^{-2}), T is the absolute temperature (K), R is the universal gas constant (8.314 J/Mol·K), C_e is the liquid phase concentration of adsorbate at equilibrium (mg/L) and β (g^2·J^{-2}) is the constant related to the mean free energy E, of sorption per mole of the sorbate as it migrates to the surface of the solid from infinite distance in the solution.

The adsorption energy, denoted as (E) (in kJ/mol), is calculated using the following equation [88]:

$$E = \frac{1}{(2\beta)^{0.5}}. \quad (46)$$

The value of E provides important information for determining the mechanism of the adsorption process (Table 2).

The Dubinin-Radushkevitch (D-R) isotherm equation has been employed to describe a variety of adsorption systems. These include the sorption of nitrogen using activated carbon, the adsorption of benzene using activated carbons, the adsorption of acid dyes using activated carbons, and the adsorption of subcritical vapors using zeolites [88, 90].

4.7. Modified Freundlich isotherm model

A number of multi-component isotherm models have been suggested to explain equilibrium adsorption data. These models include the Langmuir isotherm for multisite adsorption, the modified Freundlich model for competitive adsorption, and the Ideal Adsorption Solution Theory (IAST) model [40, 61, 92]. The commonly employed model for accurately describing equilibrium data in multi-component adsorption systems is the multi-component Freundlich isotherm. Initially proposed by Sheindorf et al. [93], this model is based on the assumption of a heterogeneous distribution of energies, which was originally used in deriving the single-component Freundlich isotherm. Also, the model considers competitive adsorption coefficients to account for the influence of other solutes (components) [94, 95]. For binary component systems, the modified Freundlich equation representing the behavior of each solute is given as [92]:

Table 2 Values of adsorption energy E indicating nature of adsorption mechanism [18].

Values of E (kJ/mol)	Information about the adsorption process
E <8	Physical adsorption
8 < E < 16	Ion exchange process
E >16	Chemical adsorption

$$q_1 = K_1C_1(C_1 + a_{12})^{\frac{1}{n_1}-1}, \quad (47)$$

$$q_2 = K_2C_2(C_2 + a_{21})^{\frac{1}{n_2}-1}. \quad (48)$$

The linearized form of Equations 47 and 48 are represented as [96]:

$$\frac{C_1}{C_2} = \frac{1}{C_2}\beta_1 - a_{12}, \quad (49)$$

$$\frac{C_2}{C_1} = \frac{1}{C_1}\beta_2 - a_{21}, \quad (50)$$

$$\beta_1 = \left(\frac{K_1C_1}{q_1}\right)^{\frac{1}{\left(1-\frac{1}{n_1}\right)}}, \quad (51)$$

$$\beta_2 = \left(\frac{K_2C_2}{q_2}\right)^{\frac{1}{\left(1-\frac{1}{n_2}\right)}}, \quad (52)$$

where a_{12} (dimensionless) is the competition coefficient of component 1 in the presence of component 2, a_{21} (dimensionless) is the competition coefficient of component 2 in the presence of component 1, (dimensionless), q_1 is the amount of component 1 adsorbed per unit mass of adsorbent (mg/g), q_2 is the amount of component 2 adsorbed per unit mass of adsorbent (mg/g), K_1 is the single component Freundlich capacity factor for component 1 $\left(\mathrm{mg}^{1-1/n}L^{1/n}\mathrm{g}\right)$, K_2 is the single component Freundlich capacity factor for component 2 $\left(\mathrm{mg}^{1-1/n}L^{1/n}\mathrm{g}\right)$, n_1 (dimensionless) is the Freundlich isotherm parameter for component 1, while n_2 (dimensionless) is the Freundlich isotherm parameter for component 2. This equation has been effectively utilized to describe the competitive adsorption behavior of organic compounds (such as p-nitrophenol and benzene sulfonate) onto activated carbon [93, 97].

5. Application of Agrowastes-derived activated carbons for dye removal

In their study, Zarzour et al. [98] developed activated carbon from various samples of the organic fraction of municipal solid waste (OFMSW) using $ZnCl_2$ as the activating agent. They investigated the impact of different impregnation ratios of $ZnCl_2$ to OFMSW (ranging from 0.2:1 to 1.5:1) on the adsorption properties of iodine and methylene blue from aqueous solutions. Their findings revealed that an impregnation ratio of 0.6:1 (corresponding to a 60% $ZnCl_2$ concentration) resulted in optimal values for the BET surface area (549.6 m^2·g^{-1}), methylene blue adsorption capacity (112.4 mg·g^{-1}), and iodine adsorption capacity (134 mg·g^{-1}). Additionally, they explored the removal of chromium (VI) ions from aqueous solutions using $ZnCl_2$-activated organic fraction municipal solid waste (OFMSW). The adsorption of chromium (VI) ions increased with higher initial concentrations (up to an optimal concentration of 70 mg·L^{-1}), longer contact times (reaching an

 DOI: 10.15826/chimtech.2024.11.2.02

optimum of 90 min), and lower pH levels, with maximum adsorption occurring at an acidic pH of 2. They postulated that the electrostatic attraction between the highly protonated adsorbent surface and the anionic radicals, which are predominant at low solution pH, contributes to the enhanced uptake of Cr (VI) ions from aqueous solutions. Furthermore, the abundance of accessible vacant adsorption sites at low initial concentrations of chromium (VI) ions also facilitated this adsorption process. Their study concluded that the optimal parameters for effective Cr (VI) removal were as follows: solution pH of 2, contact time of 90 min, initial chromium (VI) concentration of 70 mg·L^{-1}, and Cr(VI) adsorption capacity of 66.7 mg·g^{-1}. Furthermore, the experimental data aligned well with the Langmuir isotherm model, representing monolayer coverage of dye molecules on the adsorbent surface, as well as following pseudo second-order kinetics with a rate constant (k) of 16.47·10^{-3} g·mg^{-1}·min^{-1}.

Subramaniam and Ponnusamy [101] examined the removal of methylene blue dye from aqueous solutions using activated carbon derived from cashew nutshell. They employed potassium hydroxide as the activating agent. The study examined several variables, including initial dye concentration, pH, contact time, and adsorbent dosage. Batch equilibrium experiments were conducted across a range of initial dye concentrations (50 to 250 mg·l^{-1}), solution pH (2 to 10), adsorbent dosage (0.5 to 3 g·L^{-1}), and contact time (0 to 120 min). Utilizing Response Surface Methodology (RSM), the researchers optimized the experimental results to identify the ideal conditions for methylene blue dye removal, achieving an optimal pH of 6. The study revealed that dye adsorption increased linearly with higher solution pH, greater adsorbent dosage, longer contact time, and lower initial dye concentration. This enhancement was attributed to electrostatic interactions between positively charged dye ions (cations) and the negatively charged adsorbent surface as well as improved mobility of dye molecules from the bulk solution to active sites on the surface of the cashew nutshell activated carbon. Based on their findings, the recommended batch adsorption conditions were as follows: adsorbent dose of 2.1846 g, contact time of 63 min, pH of 10, and initial dye concentration of 50 mg·l^{-1}.

AlOthman et al. [102] investigated the adsorption of methylene blue using activated carbon derived from a mixture of waste materials, including polystyrene, palm tree trunks, and waste cartons. The initial concentration of the methylene blue stock solution was 1000 mg·l^{-1}. In batch mode, 0.03 grams of $ZnCl_2$-activated mixed waste carbon was combined with 80 ml of methylene blue solution. The study focused on solution pH, initial methylene blue concentration, and contact time as variables. They observed that the adsorption of methylene blue increased with longer contact time and higher initial dye concentration. Surprisingly, the amount of methylene blue adsorbed remained independent of solution pH. The removal mechanism was attributed to electrostatic interactions between the adsorbing ions and the carbon surface (physical adsorption). Notably, the adsorption process exhibited significant dependence on the initial dye concentration. Optimal conditions were achieved with initial dye concentration of 150 ppm, contact time of 480 min, and MB dye adsorption capacity of 140.03 mg·g^{-1}.

Kooh et al. [32] investigated the adsorption behavior of Malachite Green (MG) using three types of activated Azolla Pinnata: non-activated (UAP), NaOH-activated (NAP), and H_3PO_4-activated (PAP). The study involved batch equilibrium experiments with varying parameters, including temperature (25 to 65 °C), ionic strength (0 to 0.80 mol.l^{-1}), contact time (5 to 240 min), adsorbent dosage (0.01 to 0.06 g), and initial ion concentration (20 to 600 mg·l^{-1}). They observed that the adsorption of MG increased with higher adsorbent dosage, initial ion concentration, pH, temperature, and contact time, while it decreased with increasing ionic strength. Competitive adsorption by cations (Na^+ and K^+) at elevated salt concentrations inhibited MG adsorption. Additionally, pH studies revealed that mechanisms beyond physical adsorption, such as hydrogen bonding and hydrophobic interactions, contributed to MG removal on the surfaces of UAP and NAP. In contrast, PAP exhibited chemical adsorption for MG removal. Optimal pH values for MG adsorption were 5.9, 5.0, and 5.0 for NAP, PAP, and UAP, respectively. Among the activated carbons, H_3PO_4-activated Azolla Pinnata (PAP) demonstrated the highest adsorption capacity (68.3 mg·g^{-1}) for MG removal from aqueous solutions. In conclusion, PAP proved to be the most effective adsorbent for Malachite Green removal. Unfortunately, the authors did not accurately ascertain the adsorption mechanism's nature by employing the isotherm parameter. Calculating the mean free energy of adsorption per molecule of adsorbate (E) from the Dubinin-Raduskevich (D-R) isotherm equation could have significantly enhanced their research.

Kang et al. [101] conducted a study utilizing corn stalk and walnut shell as raw materials for mix-based activated carbon production. Phosphoric acid served as the activating agent, and an orthogonal experimental design resulted in nine carbon samples with varied concentrations of phosphoric acid (3 mol·L^{-1} to 5 mol·L^{-1}), mass ratios of corn stalk to walnut shell (3:7 g·g^{-1} to 7:3 g·g^{-1}), activation temperatures (300 °C to 500 °C), and activation times (1 h to 3 h). Optimization of activation conditions, including phosphoric acid concentration, mass ratio, temperature, and time, led to the preparation of mix-based H_3PO_4-activated carbon (CWAC) under specific conditions (4 mol·L^{-1}, 3:7, 400 °C, 1 h). This CWAC exhibited superior adsorption properties, with iodine number of 720.5 mg·g^{-1}, methylene blue number of 195.0 mg·g^{-1}, and surface area of 1187 m^2·g^{-1}. Characterization involved textural analysis and surface chemistry studies. They found that the mix-based activated carbon had a predominantly mesoporous architecture. Kang et al. also conducted batch studies with varying adsorption time (ranging from 0 to 140 min) and initial solution pH (ranging from 3 to 9). The adsorption data was analyzed using adsorption isotherms (specifically Langmuir and

 DOI: 10.15826/chimtech.2024.11.2.02

Freundlich models) and kinetic models (both Pseudo-first order and Pseudo-second order). Their findings revealed that malachite green adsorption onto mix-based activated carbon (CWAC) followed pseudo second-order kinetics, with a calculated kinetic rate constant (k_2) of $3.01{\cdot}10^{-4}$ g·mg^{-1}·min^{-1} and an adsorption capacity ($q_{e,cal}$) of 198.41 mg·g^{-1}. This behavior was attributed to a chemisorption process involving valency forces, either through sharing (covalent bonding) or exchanging (ionic bonding) of electrons between the dye and the mix-based activated carbon (CWAC). A comparison of malachite green adsorption capacities across various materials – raw materials, CWAC, CSAC, WSAC, and commercial activated carbons – revealed that CWAC exhibited the highest adsorption capacity of 450.78 mg·g^{-1}. This enhanced capacity can be attributed to the mesoporous nature of CWAC, which facilitates the adsorption of larger macromolecular dyes like malachite green. Further, they conducted four consecutive desorption-adsorption cycles for CWAC regeneration via filtration. Subsequently, they utilized the retained CWAC for malachite green adsorption from an initial concentration of 500 mg·L^{-1}. In a subsequent run, CWAC was regenerated a fifth time through calcination at 400 °C and then employed for malachite green adsorption. Interestingly, the percentage removal of malachite green decreased from a maximum of 80.4% to an acceptable rate of approximately 30%. These results confirm that the H_3PO_4-activated mixed corn stalk-walnut shell adsorbent (CWAC) holds promise for improved reutilization after regeneration.

Haki et al. [102] conducted a comprehensive study on the adsorption of crystal violet (CV) dye using NaOH-activated Avocado Pear Seed (NaOH-AS). The research investigated various process parameters, including contact time, initial CV dye concentration, ionic strength ($NaCl_2$ and $CaCl_2$), temperature, and pH. The adsorption data were analyzed using Langmuir, Freundlich, Pseudo-first order kinetic, Pseudo-second order kinetic, and Intraparticle diffusion models. The equilibrium data aligned well with the Freundlich isotherm model, indicating multilayer and heterogeneous (physical) adsorption. The study revealed that CV dye removal efficiency increased with higher initial dye concentration, longer contact time, elevated pH, and decreased temperature, Na^{2+}, and Ca^{2+} concentrations. Kinetic studies confirmed that the CV dye uptake followed a second-order rate equation, with calculated kinetic parameters ($Q_{e,2}$ = 78.68 mg·g^{-1}, k_2 = 0.0020 g·mg^{-1}·min^{-1}). Additionally, they employed thermodynamic modeling to determine thermochemical data, resulting in Gibb's free energy, enthalpy, and entropy values of −9.501 kJ·mol^{-1}, −33.486 kJ·mol^{-1}, and −80.487 J·mol^{-1}, respectively. The findings suggest that the CV adsorption process is spontaneous, physical, and exothermic. The primary mechanisms for CV dye removal involve electrostatic interactions between dye molecules and the NaOH-AS adsorbent surface, as well as mass diffusion through the liquid film adjacent to the adsorbent surface (external film diffusion) and within the adsorbent pores (intraparticle diffusion). Notably, the maximum adsorption capacity of NaOH-Avocado Pear Seed adsorbent for CV dye was 179.80 mg·g^{-1}. Furthermore, in successive adsorption-desorption cycles (four cycles) with NaOH-AS regeneration using HCl solution, CV dye desorption yields reached a maximum of 76.4%, demonstrating the satisfactory reusability of NaOH-Avocado Pear Seed adsorbent. In conclusion, NaOH-AS showed good potential for practical applications.

Khang et al. [103] synthesized activated carbon from cashew nut shells (CNS) to remove methylene blue (MB) dye from textile industry wastewater. They conducted experiments under varying activation conditions, including time, temperature, and pH, to determine the optimal parameters (T = 85 °C, t = 70 min, and pH = 9) for producing the activated carbons. Subsequently, they analyzed the effects of pH and initial methylene blue dye concentration using kinetic models (Webber and Morris, Pseudo-first order, Pseudo-second order, and Elovich) and adsorption isotherm models (Langmuir, Freundlich, n-layer BET, Guggenheim Anderson de Boer (GAB), and Dubinin Raduskevitch). Their findings revealed that the adsorption capacity of MB dye increased with higher solution pH and initial dye concentrations. The n-layer BET model provided a better description of MB dye adsorption onto cashew nut activated carbon, suggesting heterogeneous and multilayer (physical) adsorption on the CNS activated carbon. The maximum adsorption capacity of activated cashew nut shell for MB dye was 38.5 mg·g^{-1}. During the initial adsorption stages (0 to 100 mg·L^{-1}), the Pseudo-second order kinetic model fit the experimental data well. Subsequently, the pseudo-first order kinetic model was more suitable for the later stages of Methylene Blue (MB) dye adsorption (150 to 200 mg·L^{-1}), while the Elovich kinetic model (R^2 = 0.9986) described the final stages. These results confirmed the dependence of MB dye adsorption on initial dye concentration. The adsorption mechanism involved an adsorbate (Methylene Blue dye)-Adsorbent (A-CNS) interaction occurring on the external adsorbent surface. The researchers emphasized that inconsistencies in the best-fit kinetic model could hinder a detailed understanding of the MB dye adsorption process. Therefore, a different approach towards investigating such fluid-solid adsorption systems such as mathematical modeling and simulation should be considered.

6. Application of Agrowastes-derived activated carbons for miscellaneous pollutant removal

The research conducted by Rocha et al. [104] explored the removal of phenol from aqueous solutions using activated carbon derived from corncobs treated with phosphoric acid. Their study involved batch experiments, where they investigated various initial phenol concentrations ranging from 100 to 500 mg·L^{-1}, while maintaining an adsorbent

 DOI: 10.15826/chimtech.2024.11.2.02

concentration of 10 g·L^{-1}. The adsorption kinetics of phenol onto corncob activated carbon exhibited an initial rapid adsorption rate followed by a slower approach to equilibrium conditions over a 6-hour period. Interestingly, the Freundlich isotherm accurately described the adsorption data, suggesting multilayer and heterogeneous (physical) adsorption. The primary mechanism for phenol removal involved boundary layer diffusion in the concentration range of 100–300 mg·L^{-1}, transitioning to pore diffusion predominantly in the concentrated solution range (C1 > 300 mg·L^{-1}). They concluded that the phenol adsorption onto corncob activated carbon was considered favorable.

Walnut shells have been studied using chemical treatment and low activation temperature (450 °C) by Nazari et al. [105]. In this investigation, $ZnCl_2$ served as the activating agent, with a consistent impregnation ratio of 1:1. Their primary focus was on examining the batch adsorption behavior of Cephalexin (CFX) from aqueous solutions using $ZnCl_2$-activated walnut shell. They also developed a mathematical model to describe the batch adsorption process, emphasizing the significance of pore diffusion mechanisms. Key variables investigated included initial CFX concentration, contact time, pH, and adsorbent dosage. Through parametric studies, they found that the amount of CFX adsorbed increased with increase in adsorbent dosage and initial solution pH with a maximum adsorption capacity of 6.5 mg·g^{-1}. This enhanced Cephalexin uptake was attributed to factors such as electrostatic interactions, interference between binding sites, solute availability, and the abundant concentration of negatively charged CFX species in the solution. The optimal parameter values for initial CFX concentration, initial pH, adsorbent dosage, contact time, and Cephalexin adsorption capacity (based on the Langmuir isotherm) were identified as 200 mg·L^{-1}, 6.5, 0.6 g·L^{-1}, 20 h, and 233.1 mg·g^{-1}, respectively. Furthermore, the estimated model parameter-effective macropore diffusivity of CFX was validated through close agreement with experimental results.

In their study, Menkiti et al. [106] explored the removal of suspended and dissolved particles (SDP) from brewery effluent using Chrysophyllum albidium seed shell activated carbon. The researchers investigated various process parameters in batch mode, including biosorbent dose, pH, temperature, and contact time. Their findings revealed that SDP removal increased linearly with an increase in adsorbent dosage (optimal dose of 50 g·L^{-1}), time (optimal time of 30 min), temperature (optimal temperature of 30 °C), and pH (optimal pH value of 6.95). This enhancement was attributed to electrostatic attraction between the cationic adsorbate (BRE) molecules and the negatively charged adsorbent surface, along with improved mobility of SDP molecules from the bulk solution to vacant sites on the adsorbent surface. They concluded that the optimal conditions for adsorbent dosage, temperature, contact time, and pH were 50 g·L^{-1}, 30 °C, 30 min, and 6.95, respectively.

Zhu et al. [26] conducted a study on the adsorption of ammonium ions using activated carbon derived from avocado seeds. The avocado seeds were impregnated with 70% (by weight) methanesulfonic acid (with an impregnation ratio of 0.8:1) and then carbonized at 700 °C for 15 h. The resulting activated product underwent thorough rinsing with deionized water and subsequent drying. Subsequently, 0.3 g of avocado seed activated carbon was introduced into a 100 ml solution containing ammonium ions (NH_4^+) for a batch adsorption study. The research investigated the impact of various experimental parameters, including initial solution pH (ranging from 3 to 9), initial NH_4^+ ion concentrations (ranging from 50 to 459 mg·l^{-1}), adsorbent dosage (ranging from 1 to 20 g·L^{-1}), and contact time (ranging from 0 to 350 min), on the removal of ammonium ions from aqueous solutions using the batch method. The study revealed that the adsorption of ammonium (NH_4^+) ions increased with rising pH (reaching an optimal value at pH 5), higher adsorbent dosage, longer contact time, and greater initial adsorbate concentration. Interestingly, the equilibrium time remained unaffected by the initial sorbate concentration. The primary mechanism responsible for ammonium ion removal was attributed to strong ionic interactions between the predominantly acidic surface functional groups of the sorbent and the NH_4^+ ions. Additionally, the increased availability of NH_4^+ ions and the greater number of adsorption sites on the adsorbent surface contributed to the overall adsorption effectiveness. The maximum adsorption capacity of the avocado seed adsorbent for ammonium (NH_4^+) was determined to be 5.4 mg·g^{-1}.

The study conducted by Sellaoui et al. [107] investigated the adsorption of 3-aminophenol (3ANP) and resorcinol (RSC) from aqueous solutions using activated carbon derived from avocado seeds. The preparation involved microwave heating and $ZnCl_2$ activation. During the study, they conducted batch studies with varying initial concentrations of the phenolic compounds (ranging from 100 to 1800 mg·l^{-1}) while maintaining a fixed contact time of 480 min. To analyze the equilibrium adsorption data, they employed several statistical physics models including Multilayer model with saturation (MLMS), Monolayer model with one energy (MLIE) and Double layer model with two energies (DLM2E). Amongst these models, the monolayer model with one energy (MLIE) provided the best fit to the experimental adsorption data. The maximum adsorption capacities were determined to be 406 mg·g^{-1} for resorcinol and 455 mg·g^{-1} for 3-aminophenol. Additionally, the steric parameter was found to be less than 0.5 for both sorbates, indicating that they were bonded to the activated carbon surface in a parallel orientation. Moreover, the researchers performed a thermodynamic analysis of the adsorption data for 3ANP and RSC. The calculated values for Gibbs's free energy, enthalpy, entropy, and adsorption energy were all negative. This confirms that the adsorption of both molecules onto the avocado seed activated carbon was exergonic and spontaneous. The optimal conditions for 3ANP and RSC

 DOI: 10.15826/chimtech.2024.11.2.02

adsorption onto the avocado seed activated carbon were solution temperature of 50 °C and pH of 7, respectively.

7. Agrowastes-derived activated carbon utilization for heavy metals removal

In their study, Rahman et al. [108] investigated the removal of heavy metal ions (Ni, Pb, Cr) from aqueous solutions using activated carbon derived from two types of lignocellulosic materials: coconut shells and oil palm kernel shells. The activation process involved chemical treatment with H_3PO_4 as the activating agent, with impregnation ratios of 0.5:1 and 1:1. They studied different variables, including initial ion concentration and solution pH. For all activated carbons, individual batch equilibrium studies were conducted with varying initial concentrations of Ni(II) and Pb(II), ranging from 6 to 227 mg·l^{-1} and 50 to 600 mg·l^{-1}, respectively. The solution pH was maintained at a constant value of 5. Additionally, batch equilibrium studies were performed with varying initial concentrations of Cr(VI) ions, ranging from 40 to less than 600 mg·l^{-1}, while maintaining an initial solution pH of 3. The study revealed that the adsorption of lead (II) and Ni (II) ions increased with higher pH values above the point of zero charge (pHzpc) of the adsorbent surface (approximately 3.6±0.1 mg·g^{-1}). Conversely, the adsorption capacity decreased with increasing initial metal ion concentrations. They attributed this phenomenon to the electrostatic attraction between the negatively charged adsorbent surface and the cations (Pb^{2+} and Ni^{2+}), which facilitated the uptake of metal ions from the aqueous solutions. Regarding the efficiency of activated carbons for removing Pb(II) and Ni(II) ions at low concentrations, the order was as follows: PSW-P-ad-500 (activated palm kernel shell, impregnation ratio 0.5:1) > CPW-P-500 (coconut shell) > PSW-P-500 (activated palm kernel shell, impregnation ratio 1:1) > CAC (commercial activated carbon). Furthermore, PSW-P-ad-500 exhibited the highest Ni(II) and Pb(II) adsorption capacities, measuring 19.6 mg·g^{-1} and 74.6 mg·g^{-1}, respectively (based on the Freundlich Isotherm). They also discovered that the adsorption of Chromium (VI) ions decreased as the initial ion concentration and pH increased. At a maximum value of 20 mg·g^{-1} (pH 3), this trend was observed across all activated carbons. Their analysis indicated that the electrostatic repulsion between the negatively charged adsorbent surface and the negatively dichromate ions played a crucial role in reducing their uptake from aqueous solutions. Among the various activated carbons tested, PSW-P-ad-500 exhibited the highest efficiency for removing chromium (VI) ions, with an impressive removal efficiency of 98.9% and an adsorption capacity of 46.30 mg·g^{-1}. In addition, batch equilibrium studies were conducted to simultaneously recover three heavy metal ions (Pb, Ni, and Cr) from aqueous solutions. The selective order of metal ion adsorption by PSW-P-ad-500 was found to be Pb>Ni>>Cr, corresponding to their increasing electronegativity values (1.85, 1.854, and 1.60). The researchers concluded that PSW-P-ad-500, derived from acid-activated oil palm kernel shells, is a suitable adsorbent for efficiently removing Ni(II), Pb(II), and Cr(VI) ions at low concentrations. This finding highlights the potential of PSW-P-ad for use in drinking water purification to eliminate heavy metal contaminants.

The study conducted by Erhayem et al. [109] investigated the adsorption of mercury (Hg) using activated carbon derived from Rosmarinus officinalis leaves (referred to as ACROL). Their research involved utilizing stock solutions with mercury concentrations ranging from 100 to 400 mg·l^{-1} at a consistent pH of 2.4. Additionally, they explored temperatures between 298 K and 318 K to identify optimal adsorption conditions. Erhayem and colleagues observed that the adsorption of Hg (II) increased with rising temperature and higher initial ion concentrations. They concluded that the removal of mercury ions from aqueous solutions occurred primarily through chemical adsorption onto the ACROL material. This phenomenon was attributed to strong ionic interactions between the positively charged Hg (II) ions and the negatively charged surface of the adsorbent. The most effective conditions for Hg (II) ion adsorption onto ACROL were found to be a temperature of 318 K and an initial Hg (II) concentration of 300 mg·l^{-1}. These findings contribute to the elucidation of mercury removal processes using natural adsorbents like Rosmarinus officinalis leaves activated carbon.

Maheshwari et al. [110] investigated the adsorption of copper and zinc using activated carbon derived from neem bark through sulphuric acid treatment. The study involved two sets of simulated wastewater samples with varying initial concentrations of zinc and copper, ranging from 60 to 200 mg/l. The researchers examined the impact of process variables, including adsorbent dosage (4–40 g·L^{-1}), contact time (0–48 h), temperature (35–60 °C), and pH (1.1–12.2), on the removal of Zn(II) and Cu(II) ions individually. The results indicated that both Zn(II) and Cu(II) adsorption increased with longer contact times (up to an optimal value of 48 h), higher initial ion concentrations (up to an optimum concentration of 200 mg·l^{-1}), reduced adsorbent dosage (from an optimum dose of 6 g·L^{-1}), lower pH (from an optimum pH of 1.2), and decreased temperature (from an optimum temperature of 35 °C). The removal mechanism for Zn(II) and Cu(II) was attributed to intra-particle diffusion and film diffusion, respectively. The maximum adsorption capacities obtained for Zn(II) and Cu(II) adsorption onto neem bark activated carbon were 11.904 mg·g^{-1} and 21.23 mg·g^{-1}, respectively. The corresponding optimal values for contact time, adsorbent dosage, initial concentration, pH, and temperature were 48 h, 6 g·L^{-1}, 200 mg·l^{-1}, 1.2, and 35 °C, respectively. Furthermore, batch equilibrium studies were conducted to simultaneously recover three heavy metal ions (Zn(II), Cr(IV), and Cu(II)) from aqueous solutions. The researchers utilized an initial concentration of 200 mg·l^{-1} for each studied metal to evaluate the overall adsorption capacity of neem bark activated

 DOI: 10.15826/chimtech.2024.11.2.02

carbon. They found that the overall adsorption capacity of neem bark activated carbon, obtained for simultaneous multiple metal ion adsorption (including zinc, lead, and hexavalent chromium), was 38.95 mg·g^{-1}. This value significantly surpasses the earlier evaluations for Cu(II) (21.23 mg·g^{-1}) and Zn(II) adsorption (11.904 mg·g^{-1}). The enhanced adsorption capacity is attributed to the absence of selective affinity of the adsorption sites toward any specific metal ion. Consequently, surface binding sites remain unoccupied by any of the remaining metallic ions during the adsorption process of Zn(II), Cr(VI), and Cu(II) from aqueous solutions. They concluded that the neem bark activated carbon is a more efficient adsorbent for the removal of multiple ions from aqueous solution.

Salman et al. [111] investigated the adsorption of lead using dried diatomite, sepiolite, and dried activated carbon derived from activated sludge biomass. In their batch studies, they examined the adsorption of Pb^{2+} from aqueous solutions, considering factors such as adsorbent dosage (ranging from 1 to 20 g·L^{-1}), contact time (1 to 60 min), initial Pb^{2+} concentration (1 to 100 mg·l^{-1}), and pH (2 to 6). Their findings revealed that the uptake of lead (Pb^{2+}) ions increased with higher adsorbent dosage (optimal at 5 g·L^{-1}), elevated pH (optimal at 4), and longer contact time (optimal at 50 min). Conversely, the initial metal ion concentration had an inverse effect, resulting in decreased adsorption of lead (Pb^{2+}) ions as the concentration increased. Notably, solution pH played a critical role in batch performance, with lead removal efficiency significantly improving at higher pH levels. The primary mechanism for lead removal was attributed to electrostatic interactions between lead (II) ions in solution and the adsorbent surface, driven by Van der Waals forces (physical adsorption mechanism). In all, sepiolite derived activated carbons demonstrated the highest efficiency for removing lead (II) ions from aqueous solutions, making it a more suitable adsorbent for treating lead-contaminated wastewaters.

El-Naggar et al. [112] investigated the adsorption behavior of Cu^{2+}, Pb^{2+}, and Cd^{2+} using activated carbon produced through both physical and chemical treatments. The chemical treatment involved using activating agents such as KOH and $ZnCl_2$ on Cornocarpus Pruning waste. Consequently, two types of chemically activated carbons were generated: $ZnCl_2$-activated carbon and KOH-activated carbon, alongside the physically activated Cornocarpus waste (referred to as non-activated carbon). The stock solutions employed had concentrations of 1000 mg·L^{-1} at a fixed pH of 5.0. Batch studies explored varying initial solute concentrations (ranging from 5 to 50 mg·L^{-1}) and examined the effects of contact time and initial concentration. The results indicated that the adsorption of copper (II), lead (II), and cadmium (II) ions increased with higher initial metal ion concentrations and longer contact times. The adsorption capacities of the activated carbons for heavy metal ions followed this order: KOH-activated carbon (CK) > Non-activated carbon (CH) > $ZnCl_2$-activated carbon (CZ) > Commercial activated carbon (CC). Notably, KOH-activated carbon exhibited the highest adsorption capacities for Cu (II), Pb (II), and Cd (II), with values of 16.5, 39.5, and 21.0 μmoL·g^{-1}, respectively. Additionally, the selective order of metal ions adsorption by KOH-activated carbon was $Pb^{2+} > Cd^{2+} > Cu^{2+}$, corresponding to increasing ionic radius (0.118, 0.097, and 0.073). The adsorption mechanism for these heavy metal ions involved both chemisorption and ion exchange processes. Furthermore, batch adsorption studies explored the recovery of multiple solutes (Cd^{2+}, Pb^{2+}, and Cd^{2+}) from aqueous solutions, considering both individual (single solute) and concurrent (multi-solute) scenarios. Throughout these experiments, the solution was maintained at a constant concentration of 5.0 mg/L and pH of 5.0. They found that metal interactions played a pivotal role in the adsorption of metal ions from the multi-solute system. Each metal ion competing for available adsorption sites on the carbon surfaces. The tested adsorbents demonstrated varying efficiencies in removing heavy metal ions (Cd^{2+}, Pb^{2+}, and Cu^{2+}) from solution, with the order being CK > CH > CZ > CC. Additionally, the selective order of metal ion adsorption by KOH-activated carbon (CK) followed the sequence $Cu^{2+}>Pb^{2+}>Cd^{2+}$, based on increasing electronegativity (1.9, 1.8, and 1.7) and decreasing hydroxide solubility product ($1{\cdot}10^{-20}$, $2.5{\cdot}10^{-16}$, and $3.2{\cdot}10^{-14}$). Their findings indicated that KOH-activated carbon outperformed other activated and non-activated carbons for removing heavy metal ions from aqueous solutions. They concluded that activated conocarpus waste holds promise for effectively purifying heavy metals-contaminated wastewater.

Mise and Patil [113] conducted a study on the removal of Cr(VI) from synthetic wastewater using physically activated mango seed shells, NaCl-activated mango seed shells, and $CaCl_2$-activated mango seed shells. They investigated various experimental parameters, including adsorbent dose (ranging from 0 to 300 mg), impregnation ratio (from 0.25 to 0.75), contact time (from 0 to 60 min), and solution pH (ranging from 0 to 3.0) in batch mode. Their findings revealed that the adsorption of Cr(VI) on all the activated carbons exhibited rapid initial uptake followed by a gradual approach toward equilibrium (saturation) concentration over approximately 50 min. Moreover, they observed that Cr(VI) adsorption increased with higher adsorbent dosage, greater impregnation ratio, and lower solution pH. These trends were attributed to the increased surface area of the activated carbons, resulting in more available adsorption sites. The equilibrium data obtained from their study were well represented by the Freundlich isotherm for Cr(VI) adsorption across all the activated carbons. Notably, $CaCl_2$-activated carbon demonstrated the highest Chromium (VI) removal efficiency, achieving 90% removal. Based on these results, they recommended optimal batch adsorption conditions of impregnation ratio (0.75), pH (1.5), contact time (35 min), and adsorbent dosage (150 mg).

Siripatana et al. [114] investigated the adsorption of lead (II) using non-activated cashew nut shells (CNS). In

 DOI: 10.15826/chimtech.2024.11.2.02

their batch adsorption studies, they varied the initial ion concentrations and particle sizes, ranging from 10 to 50 mg·l^{-1} and 0.25 to 1.0 mm, respectively. They found observed that lead adsorption on CNS exhibited a rapid initial uptake followed by a gradual approach toward equilibrium (saturation) over a 4 h period. Furthermore, they noted that the percentage of lead removal increased as the initial lead (II) ion concentration decreased and the particle size decreased. To analyze the equilibrium adsorption data, they employed various kinetic models, including Pseudo-first order, Pseudo-second order, Elovich, intra-particle, and liquid-film correlations. The evaluated kinetic rate constants (k_2) fell within the range of 0.085 to 5.517 g·mg^{-1}·min^{-1}. These findings suggest that the overall lead adsorption process is simultaneously influenced by electrostatic attraction (ionic bonding) between positively charged lead (II) ions and the CNS adsorbent surface (chemisorption), as well as diffusion within the adsorbent pores (intra-particle diffusion). The maximum adsorption capacity of the cashew nut adsorbent (CNS) for lead (Pb^{2+}) adsorption was ascertained to be 1.149 mg·g^{-1}.

Nuithitikul et al. [115] investigated the removal of lead (Pb^{2+}) ions from aqueous solutions using activated cashew nut shell treated with various chemicals: H_2SO_4, HNO_3, and NaOH. Their research focus was on the adsorption capacities of these activated carbons for lead (II) ions. The study revealed that the combination of numerous surface functional groups, enlarged surface areas, and wider porosities significantly enhanced the lead adsorption capabilities of the activated carbons. H_2SO_4-activated cashew nut shell exhibited the highest lead adsorption capacity of all the tested carbons, 8.30 mg·g^{-1}. The other activated carbons followed in decreasing order: HNO_3-activated cashew nut shell (6.39 mg·g^{-1}), NaOH-activated cashew nut shell (3.22 mg·g^{-1}), and untreated cashew nut shell (2.08 mg·g^{-1}). Further, the researchers conducted batch studies to explore lead (II) ions adsorption across varying initial concentrations (ranging from 10 to 50 mg·l^{-1}). They analyzed the adsorption data using several isotherm models, including Langmuir, Freundlich, Temkin, and Dubinin-Raduskevitch, as well as kinetic models such as Pseudo-first order, Pseudo-second order, Elovich, and Intra-particle diffusion. Interestingly, the lead adsorption capacities of H_2SO_4-activated CNS exhibited a non-monotonic increase with rising initial lead ion concentration. This non-linear relationship was attributed to sorption site exhaustion at high concentrations (40 and 50 mg·l^{-1}). Moreover, the researchers found that the lead uptake rate followed both pseudo-first order and intra-particle diffusion kinetics, with calculated rate constants (k_1 and k_{int}) falling within the ranges of 0.0014 to 0.04 min^{-1} and 0.314 to 0.644 mg·g^{-1}.min^{-1}, respectively. The Langmuir isotherm provided the most accurate description of lead adsorption onto H_2SO_4-activated CNS. The results indicated that the adsorption process primarily relies on physical interactions. The highest adsorption capacity for lead (II) ions on H_2SO_4-activated CNS was determined to be 8.734 mg·g^{-1}. Consequently, Nuithitikul et al. concluded that the practicability of H_2SO_4-activated CNS in the adsorptive treatment of Pb(II)-contaminated water was promising.

8. Packed-Bed adsorption models

In a fixed-bed column, the process of fluid-solid adsorption involves several distinct steps. First, there is liquid-phase mass transfer. Next, film (external) diffusion occurs, followed by intra-pellet diffusion. Finally, we have adsorption/desorption reactions [57]. To model this behavior, researchers have developed ab-initio mathematical models for simulating packed-bed adsorption. These models incorporate parameters such as adsorption (uptake) rate, solid-liquid material balances, and equilibrium relationships (isotherms). However, due to their non-linear differential form, these models often require complex numerical methods to obtain reasonably accurate solutions. In practice, simple classical analytical models are widely used to predict the dynamic performance of packed-bed adsorption systems [116]. Some commonly employed packed-bed kinetic models include the Thomas, Yoon-Nelson, Modified Dose-Response, and Bohart-Adams models [104, 116–119].

8.1. Bohart-Adams model

Adams and Bohart [120] proposed an equation based on experimental observations related to the adsorption of chlorine using charcoal. This fundamental equation relies on the assumption of ideal plug flow and irreversible adsorption [117]. The Bohart-Adams (BA) model finds common application in describing the initial segment of the breakthrough curve (concentration-time profile) in continuous flow adsorption systems, specifically when the concentration ratio (C_e/C_0) is less than 0.15 [118]. The Bohart-Adams (BA) model can be expressed as proposed by Xu et al. [57]:

$$\frac{C_e}{C_0} = \frac{1}{1 + \exp\left(\frac{k_{BA}N_0Z}{u} - k_{BA}C_o t\right)}. \quad (53)$$

The linearized form of Equation 53 is represented as:

$$\ln\left[\frac{C_o}{C_e} - 1\right] = \ln\left[\exp\left[k_{BA}N_o\frac{Z}{u}\right] - 1\right] - k_{BA}C_o t, \quad (54)$$

where C_e is the solute concentration in the fluid phase (mg·L^{-1}), C_0 is the influent adsorbate concentration (mg·L^{-1}), N_0 is the equilibrium volumetric adsorption capacity (mg·L^{-1}), Z is the bed height (cm), t is the flow time (h), u is the linear flow velocity (cm·h^{-1}) and k_{BA} is the Bohart-Adams rate constant (Lh^{-1}·mg^{-1}).

8.2. Thomas model

In 1944, Thomas proposed a model to describe the behavior of the adsorption process in a continuous-flow (fixed bed) adsorption system. This model is derived based on second-order reaction kinetics and the Langmuir equilibrium isotherm [57, 121]. The simplified packed bed model ignores interphase (intra-particle and film diffusion) mass transfer

 DOI: 10.15826/chimtech.2024.11.2.02

and axial dispersion, implying that the adsorption process is solely controlled by surface reaction phenomena [122, 123]. The Thomas model is expressed by Equation 52, as proposed in [118] and [121]:

$$\frac{C_e}{C_o} = \frac{1}{1 + \exp\left[\frac{k_{Th}}{Q}(q_o M - C_o V)\right]}. \quad (55)$$

The linearized form of Equation 55 is represented as:

$$\ln\left[\frac{C_o}{C_e} - 1\right] = \frac{k_{Th} q_o M}{Q} - \frac{k_{Th} C_o V}{Q}, \quad (56)$$

where C_e is the effluent adsorbate concentration (mg·L^{-1}), C_o is the influent adsorbate concentration (mg·L^{-1}), q_o is the maximum solid phase concentration of the solute (mg·g^{-1}), k_{Th} is the Thomas rate constant (L·min^{-1}·mg^{-1}), V is the effluent volume (mL), Q is the volumetric flow-rate (mL·min^{-1}) and M is the mass of the adsorbent (g).

The Thomas model is widely employed to describe adsorption kinetics, evaluate model parameters (k_{Th} and q_o), and predict breakthrough curves for continuous flow (fixed-bed) adsorption systems. It is generally regarded as the optimal packed-bed model for modeling breakthrough behavior [56, 67, 117].

8.3. Yoon-Nelson model

Yoon and Nelson [124] proposed a fairly simple kinetic model for investigating the adsorption of vapors and gases onto activated coal. According to this model, the rate of decline in the likelihood of each adsorbate molecule being adsorbed is directly proportional to the probability of the adsorbate molecule's adsorption and breakthrough on the adsorbent (Kavak and Ozturk, 2004). The Yoon-Nelson model is expressed in Equation 57 [4, 117, 118]:

$$\frac{C_e}{C_o} = \frac{1}{1 + e^{K_{YN}(t-\tau)}}. \quad (57)$$

The linearized form of Equation 57 is represented as:

$$\ln\frac{C_e}{C_o - C_e} = K_{YN} t - \tau K_{YN}, \quad (58)$$

where K_{YN} is the Yoon-Nelson rate constant (h^{-1}), τ is the time required for removal of 50% of initial metal concentration (h), t is the breakthrough (sampling) time (h), C_e is the effluent sorbate concentration (mg·L^{-1}) and C_o is the initial sorbate concentration (mg·L^{-1}).

The Yoon-Nelson model is relatively straightforward compared to other kinetic models and does not necessitate extensive data on the adsorbate and adsorbent characteristics or the physical properties of the fixed-bed. However, this simplification can lead to a reduction in model accuracy when determining process variables such as exhaustion time and predicting breakthrough curves under various conditions [57, 122].

According to Chatterjee and Schiewer [117], the previously mentioned models are mathematically equivalent. Consequently, utilizing one model renders the use of other models unnecessary. The generalized model representing the Bohart-Adams, Yoon-Nelson, and Thomas models is expressed as:

$$\frac{C_e}{C_0} = \frac{1}{1 + \exp(b - at)}. \quad (59)$$

The linearized form of the generalised (BA/Th/YN) model, Equation 59, is represented as:

$$\ln\left[\frac{C_e}{C_o} - 1\right] = \ln[\exp[b] - 1] - at, \quad (60)$$

where a and b denote the lumped parameters representing the characteristics of various models (Table 3). Here, C_o represents the influent concentration in milligrams per liter (mg·l^{-1}), C_e corresponds to the effluent concentration (also in mg·l^{-1}), and t signifies the flow time in hours.

8.4. Modified dose-response model

Yan et al. [126] postulated an empirical relationship to describe metal biosorption in fixed columns based on the empirical dose-response model commonly employed in pharmacological studies. The modified dose-response model can be expressed as follows [57]:

$$\frac{C_e}{C_o} = 1 - \frac{1}{1 + \left(\frac{t}{\beta}\right)^{\alpha}}. \quad (61)$$

The linearized form of Equation 61 is represented as:

$$\ln\frac{C_e}{C_o - C_e} = \alpha \ln t - \alpha \ln \beta, \quad (62)$$

where α represents the model constant, β denotes the time at which the effluent concentration reaches 50% of the influent concentration (in hours), C_e stands for the effluent adsorbate concentration (in mg·L^{-1}), and t represents the flow time (in hours).

The modified dose-response model has found successful application in describing the adsorption of metals in diverse continuous-flow adsorption systems [127, 128].

9. Packed bed adsorption studies

Xu et al. [57] asserted that fixed bed adsorption is the primary choice for practical-scale wastewater treatment applications. Fixed-bed adsorption studies allow convenient evaluation of adsorbent performance, considering process variables such as influent concentration, adsorbent dosage (bed height), and flow rate.

The evaluation is facilitated through breakthrough curves obtained either via mathematical modeling or experimental determination [121].

Table 3 Model expressions for lumped parameters a and b in terms of packed bed model parameters [117].

Lumped parameter	Thomas (Th)	Yoon-Nelson (YN)	Bohart-Adams (BA)
a	$k_{Th}C_o$	k_{YN}	$k_{BA}C_o$
b	$k_{Th}q_{Th}M/Q$	$k_{YN}\tau$	$k_{BA}N_o Z/u$

 DOI: 10.15826/chimtech.2024.11.2.02

Column experiments more accurately represent the dynamic behavior typical of industrial wastewater treatment plant operations. Various researchers have recently conducted both numerical and experimental fixed-bed column studies to assess the performance of activated carbon adsorbents [129–131].

Garcia-Mateos et al. [33] conducted numerical studies on the adsorptive removal of paracetamol in fixed-bed columns using biomass activated carbon. Their investigation involved analyzing batch adsorption data and employing kinetic and isotherm models to determine kinetic and adsorption equilibrium parameters (K_L, D_e, q_L) necessary for predicting breakthrough profiles in a lab-scale fixed adsorption column. Additionally, they developed two distinct mathematical models for the fixed-bed column. The first model utilized a heterogeneous diffusivity coefficient approach, accounting for the dependence of diffusion on the surface coverage of paracetamol. The second model employed a constant pattern linear driving force (CP-LDF) approximation approach. Several assumptions were made, including negligible radial concentration gradients, isothermal column operation, constant axial velocity, and interparticle mass transfer characterized by an effective diffusion coefficient (D_e). Mass transport between the bulk phase and solid-particle interface was described by the external film mass transfer coefficient, k_i. Numerical solutions were obtained for the resulting ordinary differential equations (ODEs) using the finite differences method. By applying the 4^{th} order Runge-Kutta method, they determined the time-dependent paracetamol bed concentration (C_b) at the exit of the packed column. The breakthrough profiles predicted using both mass transfer resistance models (heterogeneous diffusion coefficient and CP-LDF) were validated against experimental data. Markedly, the experimental heterogeneous diffusion coefficient-based model provided the best representation of the breakthrough curve, whilst the CP-LDF model did not accurately predict the breakthrough profile. Furthermore, they estimated design parameters (Bed service time, BST, and Height of mass transfer zone, H_{MTZ}) based on the calculated and experimental breakthrough curves. They also investigated the impact of various operational parameters such as flow rate, adsorbent dosage, fixed bed length, temperature, and inlet paracetamol concentration on the performance of an adsorption column. Their findings revealed that changes in flow rate had minimal influence on the shape of the breakthrough curve, indicating the absence of external mass transfer control. Additionally, they observed that breakthrough time increased with higher adsorbent dosage, suggesting a direct correlation between breakthrough time and the amount of activated carbon used. Furthermore, at elevated temperatures, the adsorption phenomenon is characterized with higher diffusion coefficients but reduced paracetamol adsorption capacities. Interestingly, altering the adsorbent dosage had negligible impact on the breakthrough curve shape, implying the absence of adverse pressure gradients (no back-mixing) in the fixed bed column. They concluded that precise knowledge of activated carbon adsorbent performance, obtained from batch experiments, enables accurate prediction of breakthrough profiles and design parameters (such as BST and H_{MTZ}) in rapid small-scale column experiments.

Mendes et al. [132] proposed a mathematical model to predict the kinetic separation of hexane isomers and the effluent outlet composition in a fixed-bed column. Their assumptions included a non-isothermal, non-adiabatic column with axial heat dispersion, spherical adsorbent particles, linear driving force (LDF) mass transfer approximation, negligible radial temperature gradients, and a linear equilibrium relationship between the liquid and solid phases. They did not consider the effect of adsorbent particle geometry on mass and heat transfer in the solid phase. By deriving and solving material and heat balances for the target solute species and solid particles over a differential volume, they described the breakthrough behavior of the fixed-bed column. The resulting set of coupled partial differential equations was reduced to a system of ordinary differential algebraic equations (DAEs) using orthogonal collocation techniques along the spatial (Z-axis) coordinate. Solving this system of 128 DAEs involved applying a fifth-order Runge-Kutta method in conjunction with Gaussian elimination. By adjusting the residence time (t_{fb}) and the characteristic time of diffusion (t_{dif}), they explored the impact of adsorption kinetics on the model-predicted breakthrough curves. Their simulation results indicated that the separation between normal (nHex) and branched paraffins (3MP/22 DMB) is kinetically driven and can be predicted using diffusivity data from existing literature. They concluded that a proper combination of the bed residence time, $t_{fb} = L/v_i$, and the characteristic time of diffusion, $t_{dif} = 1/K_F$ (diffusivity parameters) of the (normal and branched) paraffins and gas mixtures within the adsorbent ZIF-8 fixed-bed column can lead to complete separation of hexane isomers.

Anisuzzaman et al. [133] conducted an investigation on phenol adsorption in an activated carbon packed bed column with a focus on dynamic simulation. Their study explored the dynamic behavior of phenol adsorption within a fixed-bed column containing activated carbon. By examining simulation model assumptions—specifically, convection with constant dispersion, convection with estimated dispersion, and convection with inlet liquid flow rate — they evaluated the impact on the phenol adsorption rate. The dynamic simulation was carried out using Aspen Adsorption Version 7.1. Based on their findings, the researchers concluded that the adsorption column was not a feasible choice for large-scale treatment of phenol-contaminated wastewater.

Arim et al. [134] investigated trivalent chromium biosorption onto modified pine bark in a fixed-bed column using a mechanistic model. They developed a dispersion-advection-reaction model to simulate an isothermal fixed column operation. In the proposed model, they assumed that

 DOI: 10.15826/chimtech.2024.11.2.02

the equilibrium relationship between the liquid and solid phases is described by the Langmuir isotherm, and intra-particle mass transfer is characterized by the linear driving force (LDF) approximation. The set of coupled partial differential equations derived from material balances was converted to ordinary differential equations (ODEs) using the finite difference method (truncated Taylor's series expansion). The resulting ordinary differential equations were solved through a program script implemented in the MATLAB environment. The mathematical model was demonstrated in various scenarios, including changes in bed height (H_o), superficial velocity (u_o), and initial feed concentration (C_E). In addition, they analyzed the impact of operational variables (bed depth – H_o and superficial velocity – u_o) on column performance parameters, such as the fraction of the saturated bed (FSB) and the difference between exhaustion and breakthrough time (ΔT_{abs}), using the Design of Experiments (DOE) method. Furthermore, they employed classical analytical solutions (Bohart-Adams, Yoon-Nelson, and Thomas models) for correlative modeling of the experimental data. They discovered that the classical analytical models provided a better description of trivalent chromium biosorption compared to the developed mathematical model. The inaccuracies in the model's prediction of the experimental breakthrough curve stemmed from their failure to properly account for intra-particle mass transport (diffusion effects). To address this, the classical analytical models were further adjusted using estimations of key model parameters (such as rate constants k_{yn}, k_{th}, and k_{ba}) that describe the dynamics of the continuous adsorption process. They concluded that the mechanistic model for biosorption of Cr(III) could be extended to handle other pollutants, including heavy metals and dyes.

Haroon et al. [135] synthesized five types of impregnated activated carbon through thermal pyrolysis of Eucalyptus Camaldulensis Sawdust (ECS). The ECS was pretreated with different reagents, including H_3PO_4, HCL, CH_3COOH, and H_2SO_4. These activated carbons were then evaluated for their ability to remove hexavalent chromium (Cr(VI)) using batch experiments. Amongst the synthesized materials, the H_3PO_4-activated carbon (AC-ECS) exhibited the highest chromium adsorption efficiency, exceeding 80%. Subsequently, AC-ECS was selected for further batch studies. They investigated various process parameters, including particle size, initial metal ion concentration, adsorbent dosage, contact time, temperature, pH, and column mode (bed height). Sensitivity analysis using experimental measurements helped optimize these parameters. They found that breakthrough and exhaust times increased with higher adsorbent dosage (bed height), attributed to the availability of more adsorption sites for hexavalent chromium. The bed depth service time (BDST) kinetic model was employed to analyze the data, revealing adsorption capacities of 11.353, 14.509, and 25.098 mg·l^{-1} for normalized exit solute concentrations of 0.2, 0.4, and 0.6, respectively. For full-scale column operation, the recommended operational conditions for AC-ECS were a bed height of 15 cm, an initial Cr(VI) solution concentration of 50 mg·l^{-1}, a pH of 3.0, and a flow rate of 10 mL·min^{-1}. They also explored various regeneration methods for AC-ECS, including de-ionized water, KOH, copper sulfate (CS), citric acid (CA), sulphuric acid (SA), nitric acid (NA), acetic acid (AC), ethanol (EC), phosphoric acid (PA), sodium hydroxide (NaOH), hydrochloric acid (HCL), N-hexane (NX), methanol (ML), acetonitrile (AN), ferrous sulfate (FS), ethyl acetate (EA), and acetone (AC) solutions. The highest recovery and desorption percentage of hexavalent chromium Cr(VI) from exhausted AC-ECS were 15% and 6 mg/L, respectively, using KOH solution. The observed low values for adsorbate recovery (regeneration) indicate that the adsorption process is chemical and irreversible in nature. They concluded that scaling-up the use of AC-ECS adsorbent to column lengths, as encountered in environmental engineering applications for remediating hexavalent chromium-contaminated groundwater, is an efficient treatment strategy.

Antil et al. [136] conducted fixed-bed column experiments using rice husk as an adsorbent to optimize the removal of arsenite ions from aqueous solutions. Their study investigated the impact of bed depth (adsorbent dosage), initial metal ion concentration, and flow rate on the process of arsenite adsorption by rice husk. To estimate model parameters, they employed a correlative modeling approach, fitting the Bed Depth Service Time (BDST) and Bohart-Adams (BA) kinetic models to experimental breakthrough curves. They also applied Michael and Hutchin's equations to determine adsorption bed parameters (t_Z, h_Z, V_Z, and % bed saturation). They observed that breakthrough time (the point when 10% of influent concentration is detected in the effluent) increased with decreasing flow rate, increasing bed depth, and decreasing initial concentration of arsenite ions. The decrease in rice husk adsorption efficiency at higher initial ion concentrations was attributed to increased competition among adsorbed molecules for unoccupied binding sites on the adsorbent surface. Furthermore, the Bohart-Adams kinetic model demonstrated excellent agreement with both experimental and literature values. The corresponding optimum process parameters were determined as bed depth (60 mm), flow rate (20 mL·min^{-1}), and influent concentration (50 mg·l^{-1}). The maximum arsenite adsorption capacity of the fixed-bed column was found to be 4.5 mg·g^{-1}. They concluded that the column study proved rice husk to be a potential and efficient adsorbent for the adsorption of arsenite.

Yahya et al. [14] conducted a study in which they synthesized and characterized sulphuric acid (H_2SO_4)-activated cashew nut-shell for the purpose of adsorbing hexavalent chromium (Cr^{6+}) and manganese (Mn^{2+}) ions from electroplating wastewater using a column method. To analyze the adsorption process, they employed experimental breakthrough curves under varying operational conditions, including flow-rate, influent concentration, and bed depth. The Yoon-Nelson, Adams-Bohart, and Clark

 DOI: 10.15826/chimtech.2024.11.2.02

kinetic models were fitted to the data. The Yoon-Nelson model provided the best fit to the experimental breakthrough curves, with the lowest residual sum of square errors (SSE). They discovered that the breakthrough time, exhaustion time, percentage removal, and adsorption capacities for both Mn^{2+} and Cr^{6+} ions were influenced by factors such as initial metal ion concentration, bed height, and flow-rate. These effects were attributed to shorter contact times, increased availability of vacant adsorption sites (due to a larger surface area), and intensified competition among metal ions for binding sites on the adsorbent surface. The maximum adsorption capacities of H_2SO_4-activated cashew nutshell (HCNS) were 10.79 $mg \cdot g^{-1}$ for Cr(VI) and 9.82 $mg \cdot g^{-1}$ for Mn(II) ions. This indicated that Cr(VI) adsorption was more favorable than Mn(II) adsorption in the HCNS adsorbent fixed-bed column. The primary mechanism for adsorption of Mn^{2+} and Cr^{6+} ions in the fixed-bed column was electrostatic attraction between the positively charged carbonyl and hydroxyl surface groups of the CNS adsorbent and the dissociated metallic ions. They concluded that activated cashew nut shell (HCNS) is a suitable adsorbent for removal of hexavalent chromium and manganese ions from electroplating wastewater.

From the examination of literature, it is evident that packed bed columns are increasingly utilized for industrial (practical) scale wastewater treatments. However, there is still room for improved column performance because a lot of the analytical models utilized for predicting the breakthrough curves essential for column design have not been able to elucidate the fixed bed adsorption process entirely. Typically, experimental studies also involve several time-consuming and expensive screening tests for evaluating adsorbent performances in the fixed column. Numerical modeling offers a cheaper and effective option for assessing the quality of adsorbent as well as the design and scale-up of industrial adsorptive separation processes. There are two main categories of numerical models, namely, physics-based and data-driven (black-box) models. Physics-based models are developed considering the basic physical principles and underlying theoretical knowledge. These models are useful for gaining insight into the underlying physics of the physical system. Notwithstanding, most real-life systems are complex, non-linear in nature, and contain unknown parameters that may not be possible to consider in the physical model [137]. Data-driven models can be used as substitutes for ab-inito models to describe complex physical systems. Amongst the data driven techniques, Artificial Neural Networks (ANN) is preferred due to its ability to unravel the intrinsic pattern within a group of experimental observations (linear/non-linear function approximation) without need of expert knowledge of the problem domain. An Artificial Neural Network (ANN) is a non-linear mapping of output dataset corresponding to a definite input pattern in the region of interest [138, 139]. ANN comprises of a number of simulated information processing elements (neurons) connected together to form a neural network. Artificial neural networks have become a widely utilized tool in area of process modeling, and simulation due to their inherent advantages of low computational demand, adaptability, non-linearity and noise tolerance [139]. Nonetheless, the problems associated with ANN technique include likelihood of network overtraining (over-fitting), network convergence at local minima, and the empiric process colligated with user-led specification of network architecture. A novel polynomial-type neural network that circumvents the drawbacks associated with standard ANN is the group method of data-handling (GMDH) [140]. GMDH utilizes mathematical models and numerical methods for computer-based modeling of experimental data characterized by fully automated determination of model structure, network architecture and parametric model optimization [141, 142]. GMDH is a novel tool in the area of process analysis, modeling and optimization [143]. Recently, data-driven models such as ANN have been successfully applied in the optimization of chemical processes [144–151]. However, ANN has seldom seen application for optimization of batch and continuous-flow adsorption processes. Likewise, the GMDH method has never been applied in the modeling and optimization of adsorption separation (batch and fixed-bed) processes. Soft computing techniques (i.e., GMDH and ANN method) will facilitate modeling and optimization of complex and difficult to understand processes such as fixed-bed adsorption systems without the need of human cognition.

10. Conclusion

From the literature surveys undertaken, it can be concluded that adsorption using activated carbons is an effective option for treatment of contaminated wastewaters. However, the high cost of commercially activated carbons is a limiting factor in their application for wastewater treatment. Hence, there is need for low-cost alternatives derived from abundant, readily available agricultural waste materials. Further, the adsorption capacities, kinetic and adsorption equilibrium parameters calculated using equilibrium adsorption data are normally overestimated due to attainment of equilibrium conditions (contact time) that is typically not observed in practical-scale applications [6]. Consequently, fixed-bed column studies are essential for design and scale-up of continuous (flow) adsorption systems at industrial-scale. Moreover, fixed-bed column utilization studies for evaluating adsorbent performance are still in its nascent stages. Therefore, it is important that fixed-bed column studies are paid more attention in future works pertaining to treatment of contaminated effluents.

Noteworthy, numerical (mathematical and machine learning) studies for modeling and simulation of activated carbon adsorbent batch/fixed-column system have seldom been conducted. The processes involved in the retention of adsorbate onto the adsorbent (adsorption mechanisms) and adsorption rates (kinetic effects) differ contingent on the

 DOI: 10.15826/chimtech.2024.11.2.02

individual (distinct) batch/fixed-bed column adsorption system. Hence, there is necessity to simulate the static (batch) and continuous fixed-bed columns on a case-by-case basis to evaluate the adsorption performance of the activated carbon adsorbents. The substantial loss of adsorbent capacity during regeneration is another factor limiting the application of locally activated carbons for wastewater treatment. It is important, that numerical regeneration studies are performed to effectively remove the adsorbed pollutants from exhausted activated carbons to determine desorption efficiencies and effective regeneration times for restoration of initial carbon activity.

11. Abbreviations

GMDH – Group Method of Data Handling
ANN – Artificial Neural Network
AC – Activated Carbon
BA – Adams-Bohart Model

• Supplementary materials

No supplementary materials are available.

• Funding

This research had no external funding.

• Acknowledgments

None.

• Author contributions

Conceptualization: K.V.O.
Data curation: K.V.O.
Formal Analysis: K.V.O.
Funding acquisition: K.V.O.
Investigation: K.V.O.
Methodology: K.V.O.
Project administration: J.T.N.
Resources: K.V.O.
Supervision: J.T.N.
Writing – original draft: K.V.O.
Writing – review and editing: K.V.O., J.T.N., W.P.E.

• Conflict of interest

The authors declare no conflict of interest.

• Additional information

Author ID:
Karinate Valentine Okiy, Scopus ID 57189040293.

Websites:
Nnamdi Azikiwe University, https://unizik.edu.ng/;
Federal Polytechnic Nekede, https://fpno.edu.ng/.

References

1. McCabe WL, Smith JC, Harriott P. Unit operations of chemical engineering. 5th ed. New York: McGraw-Hill; 2005. 1130 p.
2. Geankoplis, C. J. Transport processes and unit operations. 3rd ed. New Jersey: PTR Prentice Hall. 1993. 921 p.
3. Bahadir T, Bakan G, Altas L, Buyukgungor H. The investigation of lead removal by biosorption. An application at storage battery industry wastewaters. Enzyme Microb Technol. 2007;41(1–2):98–102. doi:10.1016/j.enzmictec.2006.12.007
4. Nwabanne JT, Igbokwe PK. Adsorption performance of packed bed column for the removal of Lead (II) using oil palm fibre. Int J Appl Sci Technol. 2012;2(5):106–114.
5. Adsorbers. Visual encyclopedia of chemical engineering equipment [Internet] [cited 2024]. Available from: https://encyclopedia.che.engin.umich.edu/adsorbers, Accessed on 12 January 2024
6. Zulfadhly Z, Mashitah MD, Bhatia S. Heavy metals removal in fixed-bed column by the macrofungus Pycnoporus sanguineus. Env Pol. 2001;112(3):463–470. doi:10.1016/S0269-7491(00)00136-6
7. Kafshgari F, Keshtkar AR, Mousavian MA. Study of MO(VI) removal from aqueous solution. Application of different mathematical models to continuous adsorption data. Iran J Environ Sci Eng. 2010;10(1):1–11. doi:10.1186/1735-2746-10-14
8. Barros DMAS, Arroyo PA, Silva EA. (2013). General aspects of aqueous sorption process in fixed beds. In Nakajima H. Mass Transfer-Advances in sustainable energy and environment oriented numerical modeling. 1st ed. InTech. 2013. doi:10.5772/519541
9. Ferrarezzi CG, Guirardello R. Simulation of fixed-bed adsorption column with axial particle diameter profile for removal of solutes at low concentration. Brazil J Chem Eng. 2022;39(3):743–758. doi:10.1007/s43153-021-00168-5
10. Nouh SA, Lau KK, Shariff AM. Modeling and simulation of fixed bed adsorption column using in tegrated CFD approach. J Appl Sci. 2010;10(24):3229–3235. doi:10.3923/jas.2010.3229.3235
11. Mesfer MKA, Danish M, Khan MI, Ali IH, Hasan M, Jery AE. Continuous fixed bed CO_2 adsorption: Breakthrough, column efficiency, mass transfer zone. Processes. 2020;8(10):1233–1249. doi:10.3390/pr8101233
12. Jani Y. Adsorption: A cost-effective wastewater treatment technology for removal of conventional and emerging organic contaminants. Ist ed. Cham: Springer International Publishing. 2022;118:17–33. doi:10.1007/698_2022_867
13. Ganjoo R, Sharma S, Kumar A, Daouda MMA. Activated carbon: fundamentals, classification, and properties. In Verma C, Qurashi MA. 1st eds. London: Royal Society of Chemistry; 2023. 22 p.
14. Yahya MD, Abubakar H, Obayomi KS, Iyaka YA, Suleiman B. Simultaneous and continuous biosorption of Cr and Cu(II) ions from industrial tannery effluent using almond shell in a fixed bed column. Res Eng. 2020;6:100–113. doi:10.1016/j.rineng.2020.100113
15. Abd AA, Othman MR, Kim J. A review on application of activated carbons for carbon dioxide capture: Present performance, preparation, and surface modification for further improvement. Env Sci Pol Res.2021;28(32):43329–43364. doi:10.1007/s11356-021-15121-9
16. Huang YT, Lee LC, Shih MC. A study on the pseudo-second-order kinetic equation for the adsorption of methylene blue onto nitric acid-treated rice Husk: Comparison of linear Methods. Int J of Sci and Res Pub. 2018;8(6): 7865–7877. doi:10.29322/IJSRP.8.6.2018.p7865
17. Liu W, Qi M, Chu X, Peng S, Han D. Investigation of adsorption-diffusion behaviors of elementary O_2, CO_2, and N_2 in coal particles: Influence from temperature. Env Sci Pol Res.2023;30(32):78619–78631. doi:10.1007/s11356-023-7949-4
18. Tran HN, You SJ, Chao HP. (2016). Thermodynamic parameters of cadmium adsorption onto orange peel calculated from

various methods: A comparison study. J Env Chem Eng. 2016;4(3):2671–2682. doi:10.1016/j.jece.2016.05.009
19. Yang X, Wan Y, Zheng Y, He F, Yu Z, Huang J, Wang, H, Ok YS, Jiang Y, Gao B. Surface functional groups of carbon-based adsorbents and their roles in the removal of heavy metals from aqueous solutions: A critical review. Chem Eng J 2021;366;608–621. doi:10.1016/j.cej.2019.02.119
20. Dutta S, Gupta B, Srivastava SK, Gupta AK. Recent advances on the removal of dyes from wastewater using various adsorbents: A critical review. Mater Adv. 2021;2(14):4497–4531. doi:10.1039/D1MA00354B
21. Suzuki M. Adsorption engineering. 1st ed. Amsterdam: Elsevier. 1990. 295 p.
22. Slejko FL. Adsorption technology: A step-by-step approach to process evaluation and application. 1st ed. New York: M.Dekker. 1985. 223 p.
23. Marsh H, Rodríguez-Reinoso F. Activated carbon. 1st ed. Amsterdam: Elsevier. 2006. 536 p.
24. Lima ÉC, Adebayo, MA, Machado, FM. Kinetic and equilibrium models of adsorption. In Bergmann CP, Machado FM. Carbon nanomaterials as adsorbents for environmental and biological applications [Internet]. [Cited 2024]:33–69. Available from: https://link.springer.com/10.1007/978-3-319-18875-1_3, Accessed on 14 February 2024.
25. Dotto GL, Salau NPG, Piccin JS, Cadaval TRS, de Pinto LAA. Adsorption kinetics in liquid phase: Modeling for discontinuous and continuous systems. In Bonilla- Petriciolet A, Mendoza-Castillo DI, Reynel-Ávila HE. Adsorption processes for water treatment and purification. 1st ed. Cham:nSpringer International Publishing. 2017:53–76. Available from: http://link.springer.com/10.1007/978-3-319-58136-1_3, Accessed on 14 February 2024.
26. Zhu Y, Kolar, P, Shah SB, Cheng JJ, Lim PK. Avocado seed-derived activated carbon for mitigation of aqueous ammonium. Ind Crops Prod. 2016;92:34–41. doi:10.1016/j.indcrop.2016.07.016
27. Liu G, Dai Z, Liu X, Dahlgren RA, Xu J. Modification of agricultural wastes to improve sorption capacities for pollutant removal from water-a review. Carbon Res. 2022;1(1):25–49. doi:10.1007/s44246-022-00025-1
28. Ruthven, DM, Kärger J, Brandani S, Mangano E. Sorption kinetics: Measurement of surface resistance. Adsorption. 2021;27(5):787–799. doi:10.1007/s10450-020-00257-w
29. Wang J, Guo X. Review on the intra-particle diffusion adsorption kinetics model: Interpretation, solving methods and applications. SSRN J. 2022. Available from: https://www.ssrn.com/abstract=4120203, Accessed on 14 February 2024.
30. Boyd G, Adamson A, Myers L. The exchange adsorption of ions from aqueous solutions by organic zeolites. II kinetics. J Am Chem Soc.1947;69:2836–2844. doi:10.1021/ja01203a066
31. Viegas, RMC, Campinas M, Costa H, Rosa MJ. How do the HSDM and Boyd's model compare for estimating intraparticle diffusion coefficients in adsorption processes. Adsorpt. 2014;20(5–6):737–46. doi:10.1007/s10450-014-9617-9
32. Kooh MRR, Lim LBL, Lim LH, Bandara JMRS. Batch adsorption studies on the removal of malachite green from water by chemically modified Azolla pinnata. Des Wat Tr. 2015;57(31):1–13. doi:10.1080/19443994.2015.1065450
33. García-Mateos FJ, Ruiz-Rosas R, Marqués MD, Cotoruelo LM, Rodríguez-Mirasol J, Cordero T. Removal of paracetamol on biomass-derived activated carbon: Modeling the fixed bed breakthrough curves using batch adsorption experiments. Chem Eng J. 2015;279:18–30. doi:10.1016/j.cej.2015.04.144
34. Queiroz V, de Almeida DS, de Oliveira Miglioranza GH, Steffani E, Barbosa-Coutinho E, Schwaab M. Analysis of commonly used batch adsorption kinetic models derived from mass transfer-based modelling. Environ Sci Pollut Res. 2022;29(53):79875–79889. doi:10.1007/s11356-021-18479-y
35. Rout DR, Jena HM. Removal of phenol from aqueous solution using reduced graphene oxide as adsorbent: Isotherm, kinetic, and thermodynamic studies. Environ Sci Pol Res. 2022;29(21):32105–321119. doi:10.1007/s11356-021-17944-y
36. Obradovic B. Guidelines for general adsorption kinetics modeling. Hemijska Industrija [Industrial chemistry]. 2020;74(1):65–70. Russian. doi:10.2298/HEMIND2002010060
37. Zamri NII, Zulmajdi SLN, Daud NZA, Mahadi AH, Kusrini E, Usman A. Insight into the adsorption kinetics, mechanism, and thermodynamics of methylene blue from aqueous solution onto pectin-alginate-titania composite microparticles. SN Appl Sci. 2021;3(2):1–16. doi:10.1007/s42452-021-04245-9
38. Matthews AP, Weber WJJ. Effects of external mass transfer and intra-particle diffusion on adsorption rates in slurry reactors. AIChE Sym Ser. 1976;166:91–107.
39. Qiu Y, Zheng Z, Zhou Z, Sheng GD. Effectiveness and mechanisms of dye adsorption on a straw-based biochar. Bioresource Technol. 2009;100(21):5348–5351. doi:10.1016/j.biortech.2009.05.054
40. Kwon S. Biological pretreatment of produced water for reuse applications[dissertation]. Texas (United States of America): University of Texas at Austin; 2007. 191 p.
41. Cerutti JH, Parter SV. Collocation methods for parabolic partial differential equations in one space dimension. Numerische Mathematik [Numerical mathematics]. 1976;26(3):227–254. doi:10.1007/BF01395944
42. Musah M, Azeh Y, Mathew J, Umar M, Abdulhamid, Z, Muhammad A. Adsorption Kinetics and Isotherm Models: A review. CaJoST.2022;4(1):20–26. doi:10.4314/cajost.v4i1.3
43. Kreuzer HJ. Kinetics of adsorption, desorption and reactions at surfaces. In Rocca M, Rahman TS, Vattuone L. Springer Handbook of Surface Science. 1st ed. Cham: Springer International Publishing; 2020:1035–1052. doi:10.1007/978-3-030-46906-1_31
44. Islam MA, Chowdhury MA, Mozumder MdSI, Uddin MdT. Langmuir adsorption kinetics in liquid media: Interface reaction model. ACS Omega. 2021;6(22):14481–14492. doi:10.1021/acsomega.1c01449
45. Yuh-Shan H. Citation review of Lagergren kinetic rate equation on adsorption reactions. Scientometrics. 2004;59(1):171–177. doi:10.1023/B:SCIE.0000013305.99473.cf
46. Belcaid A, Beakou BH, Bouhsina S, Anouar A. Insight into adsorptive removal of methylene blue, malachite green, and rhodamine B dyes by cassava peel biochar (Manihot esculenta Crantz) in single, binary, and ternary systems: Competitive adsorption study and theoretical calculations. Biomass Conver Bioref. 2022;12(1):1–22. doi:10.1007/s13399-022-02928-w
47. Gayathiri M, Pulingam T, Lee KT, Mohd Din AT, Kosugi A, Sudesh K. Sustainable oil palm trunk fibre based activated carbon for the adsorption of methylene blue. Sci Rep. 2023;13(1):22137–22151. doi:10.1038/s41598-023-49079-0
48. Saravanan A, Yaashikaa PR, Kumar PS, Yuvaraj D, Karishma S, Muthu CMM, Nasrin MRT, Sree GA, Karthik V, Natrayan L, Rangasamy G. Adsorption performance and modelling of malachite green dye removal from aqueous solution using sulphuric acid–modified Ipomoea pes caprae biomass. Biomass Conv Bioref. 2023;13(16):15227–15309. doi:10.1007/s13399-023-05067-y
49. Ho YS, Wase DAJ, Forster CF. Kinetic studies of competitive heavy metal adsorption by sphagnum peat. Environ Tech. 1996;17:71-77. doi:10.1080/09593331708616362
50. Plazinski W, Dziuba J, Rudzinski W. Modeling of sorption kinetics: The pseudo-second order equation and the sorbate intraparticle diffusivity. Adsorpt. 2013;19(5):1055–1064. doi:10.1007/s10450-013-9529-0
51. Shahwan T. Sorption kinetics: Obtaining a pseudo-second order rate equation based on a mass balance approach. J Environ Chem Eng. 2014;2(2):1001–1006. doi:10.1016/j.jece.2014.03.020
52. Robati D. Pseudo-second-order kinetic equations for modeling adsorption systems for removal of lead ions using multi-

walled carbon nanotube. J Nanostruct Chem. 2013;3(1):55–61. doi:10.1186/2193-8865-3-55
53. Hung YT, Holloman K. Agricultural waste as a low-cost adsorbent. In Wang LK, Wang MHS, Hung YT. Integrated Natural Resources Research. 1st ed. Cham: Springer International Publishing. 2021;22:103–146. doi:10.1007/978-3-030-61002-9_4
54. Zeldowitsch J.Über den mechanismus der katalytischen oxydation von CO and MnO_2. Acta Physicochemical URSS. 1934;1:364-449. Russian.
55. Vargas-Rodríguez MY, Obaya A, García-Petronilo EJ, Vargas-Rodríguez IG, Gómez-Cortés A, Tavizón G, Chávez-Carvayar AJ. Adsorption studies of aqueous solutions of methyl green for halloysite nanotubes: Kinetics, isotherms, and thermodynamic parameters. Am J Nanomater. 2021;9(1):1–11. doi:10.12691/ajn-9-1-1
56. Ritchie AG. Alternative to the elovich equation for the kinetics of adsorption of gases on solids. J Chem Soc. 1977;73(0):1650. doi:10.1039/f19777301650
57. Xu Z, Cai J, Pan B. Mathematically modeling fixed-bed adsorption in aqueous systems. J Zhejiang Univ Sci A. 2013;14(3):155–176. doi:10.1631/jzus.A1300029
58. Solangi ZA, Bhatti I, Qureshi K. A combined CFD-response surface methodology approach for simulation and optimization of arsenic removal in a fixed bed adsorption column. Processes. 2022;10(9):1730–1747. doi:10.3390/pr10091730
59. Piccin JS, Cadaval TRS, de Pinto LAA, Dotto GL. Adsorption Isotherms in Liquid Phase: Experimental, Modeling, and Interpretations. In Bonilla-Petriciolet A, Mendoza-Castillo DI, Reynel-Ávila HE. Adsorption Processes for Water Treatment and Purification. 1st eds. Cham: Springer International Publishing. 2017;19–51. doi:10.1007/978-3-319-58136-1_2
60. Amrhar O, El Gana L, Mobarak M. Calculation of adsorption isotherms by statistical physics models: A review. Environ Chem Lett. 2021;19(6):4519–4547. doi:10.1007/s10311-021-01279-8
61. Limousin G, Gaudet JP, Charlet L, Szenknect S, Barthes V, Krimissa M. Sorption isotherms: A review on physical bases, modeling and measurement. Appl Geochem. 2007;22:249–274. doi:10.1016/j.apgeochem.2006.09.010
62. Grassi M, Kaykioglu G, Belgiorno V, Lofrano G. Emerging Compounds Removal from Wastewater. In Green Chemistry for Sustainability, 15–38. Haz Mater. 2012;136(3):791–799. doi:10.1007/978-94-007-3916-1
63. Tadros T. (2013). Adsorption Isotherm. In Tadros T. Encyclopedia of Colloid and Interface Science. 1st eds. Berlin Heidelberg: Springer. 2013. 202 p. doi:10.1007/978-3-642-20665-8_46
64. Abin-Bazaine A, Campos Trujillo A, Olmos-Marquez M. Adsorption Isotherms: Enlightenment of the Phenomenon of Adsorption. In M. Ince M, Kaplan OI. 1st eds. Wastewater Treatment. IntechOpen. 2022:1–16. doi:10.5772/intechopen.104260
65. Ayawei N, Ebelegi AN, Wankasi D. Modelling and interpretation of adsorption isotherms. J Chem. 2017;2017:1–11. doi:10.1155/2017/3039817
66. Erdogan FO. Freundlich, Langmuir, Temkin, DR, Harkins-Jura Isotherm Studies on the Adsorption of CO_2 on Various Porous Adsorbents. Int J Chem React Eng. 2019;17(5):1542–1580. doi:10.1515/ijcre-2018-0134
67. Akinbiyi OA. Removal of Lead from Aqueous Solutions by Adsorption using Peat Moss[thesis]. Regina (Canada): University of Regina; 2000. 101 p.
68. Demirbas E, Kobya M, Konukman AES. Error analysis of equilibrium studies for the almond shell activated carbon adsorption of Cr(VI) from aqueous solutions. J Haz Mater. 2008;154:787–794. doi:10.1016/j.jhazmat.2007.10.094
69. Ajemba RO. Thermodynamics and kinetic modeling of the dissolution and adsorptive applications of Ukpor, Udi, and Nteje clays[dissertation]. Anambra (Nigeria). Nnamdi Azikiwe University, 2012. 368 p.
70. Hall KR, Egleton LC, Acrivos A, Vemeulen T. Pore and solid diffusion kinetics in fixed bed adsorption under constant pattern conditions. Indus Eng Chem Fund. 1966;5(2): 212–223. doi:10.1021/i160018a011
71. Hu K, Zhang Q, Liu Y, Thaika MA. A developed dual-site Langmuir model to represent the high-pressure methane adsorption and thermodynamic parameters in shale. Inter J Coal Sci Technol. 2023;10(1):59. doi:10.1007/s40789-023-00629-x
72. Lohrentz L, Bhaumik M, Brink HG. High-capacity adsorption of hexavalent chromium by a polyaniline-Ni(0) nanocomposite adsorbent: Expanding the Langmuir-Hinshelwood kinetic model. J Molec Liquids. 2023;389:1–14. doi:10.1016/j.molliq.2023.122931
73. Brandani S. On adsorption azeotropy and a classification based on the dual site Langmuir isotherm. Adsorpt. 2023;1–9. doi:10.1007/s10450-023-00430-x
74. Freundlich H. Over the adsorption in solution. J Phys Chem. 1906;57:385–470.
75. Burke GM, Wurster DE, Buraphacheep V, Berg MJ, Veng-Pedersen P, Schottelius DD. Model selection for the adsorption of phenobarbital. Pharm Res. 1991;8(2):228–231. doi:10.1023/a:1015800322286
76. Adamson AW, Gast AP. Physical chemistry of surfaces. New York:Wiley & Sons; 1997. 765 p.
77. Vigdorowitsch M, Pchelintsev A, Tsygankova L, Tanygina E. Freundlich Isotherm: An Adsorption Model Complete Framework. Appl Sci. 2021;11(17):8078. doi:10.3390/app11178078
78. Van der Bruggen B, Enrico D, Lidietta G. Freundlich Isotherm. In Drioli E, Giorno L. Encyclopedia of Membranes .1st eds. Berlin Heidelberg: Springer. 2016. 834–835. doi:10.1007/978-3-662-44324-8_254
79. Melvin SS, Abigail MEA, Chidambaram R. Isotherm modelling, kinetic study and optimization of batch parameters using response surface methodology for effective removal of Cr(VI) using fungal biomass. PLOS One. 2015;10(3):1–13. doi:10.1371/journal.pone.0116884
80. Khayyun TS, Mseer AH. Comparison of the experimental results with the Langmuir and Freundlich models for copper removal on limestone adsorbent. Appl Water Sci. 2019;9(8):1–8. doi:10.1007/s13201-019-1061-2
81. Temkin MJ, Pyzhev V. Kinetics of ammonia synthesis on promoted iron catalysts. Acta Physiochimica URSS. 1940;12:217–224.
82. Hansen JB. Kinetics of Ammonia Synthesis and Decomposition on Heterogeneous Catalysts. In A. Nielsen A, Ammonia. 1st eds. Berlin Heidelberg: Springer. 1995:149–190. doi:10.1007/978-3-642-79197-0_4
83. Khandelwal A, Narayanan N, Varghese E, Gupta S. Linear and nonlinear isotherm models and error analysis for the sorption of kresoxim-methyl in Agriultural Soils of India. Bull Environ Contam Toxicol. 2020;104(4):503–510. doi:10.1007/s00128-020-02803-2
84. Mabuza M, Premlall K, Daramola MO. Modelling and thermodynamic properties of pure CO_2 and flue gas sorption data on South African coals using Langmuir, Freundlich, Temkin and extended Langmuir isotherm models. Int J Coal Sci Technol. 2022;99(1):1-15. doi:10.1007/s00128-020-02803-2
85. Harkins WD, Jura EJ. The decrease of free surface energy as a basis for the development of equations for adsorption isotherms; and the existence of two condensed phases in films on solids. J Chem Phys. 1944;12:112–113. doi:10.1063/1.1723913
86. Shanavas S, Kunju AS, Varghese HT, Panicker CY. Comparison of Langmuir and Harkins-Jura adsorption isotherms for the determination of surface area of solids. Orien J Chem. 2011;27(1):245–252. Available from: http://www.orient-jchem.org/?p=24831
87. Kausar A, Bhatti HN, MacKinnon G. Equilibrium, kinetic and thermodynamic studies on the removal of U(VI) by low-cost agricultural waste. Colloids Surfaces B Biointerfaces. 2013;111:124–133. doi:10.1016/j.colsurfb.2013.05.028

88. Hutson ND, Yang RT. Theoretical basis for the Dubinin-Radushkevitch (D-R) adsorption isotherm equation. Adsorption. 1997;3(3):189–195. doi:10.1007/BF01650130
89. Saeidi N, Parvini M. Accuracy of Dubinin-Astakov and Dubinin-Raduchkevic adsorption isotherm models in evaluating micropore volume of bontonite. Period Polytech Chem Eng. 2015;60(2):123–129. doi:10.3311/PPch.8374
90. Nguyen C, Do DD. The Dubinin-Raduskevich equation and the underlying microscopic adsorption-desorption. Carbon. 2001;39:1327–1336. doi:10.1016/S0008-6223(00)00265-7
91. Hu Q, Zhang Z. Application of Dubinin–Radushkevich isotherm model at the solid/solution interface: A theoretical analysis. J Molec Liquids. 2019;277:646–648. doi:10.1016/j.molliq.2019.01.005
92. Amrutha, Jeppu G, Girish CR, Prabhu B, Mayer K. Multi-component adsorption isotherms: Review and modeling studies. Environ Processes. 2023;10(2):1–52. doi:10.1007/s40710-023-00631-0
93. Sheindorf C, Rehbun M, Sheintuch M. A Freundlich type multicomponent isotherm. J Coll Inter Sci. 1981;79:136–142. doi:10.1016/0021-9797(81)90056-4
94. Abdehagh N, Tezel FH, Thibault J. Multi-component adsorption modeling: Isotherms for ABE model solutions using activated carbon F-400. Adsorpt. 2016;22(3):357–370. doi:10.1007/s10450-016-9784-y
95. Hilbrandt I, Lehmann V, Zietzschmann F, Ruhl AS, Jekel M. Quantification and isotherm modelling of competitive phosphate and silicate adsorption ontomicro-sized grazular ferric hydroxide. RSC Adv. 2019:9(41):23642–23651. doi:10.1039/C9RA04865K
96. Sursala S. Adsorption-desorption characteristics of phenoxyacetic acids and chlorophenols in a volcanic soil [dissertation]. New Palmerston(New Zealand); 1994. 228 p.
97. Wu J, Xie Z, Guo K, Claesson O. Measurement and prediction of the adsorption of binary mixtures of organic vapours on activated carbon. Adsorp Sci Technol. 2001;19(9):737–749. doi:10.1260/0263617011494547
98. Zarzour M, Ensafi AA, Rezaei B. Preparation of activated carbon from organic fraction of municipal solid wastes by $ZnCl_2$ activation method and use it for elimination of chromium(VI) from aqueous solutions. J Iran Chem Soc. 2014;11(4):1075–1083. doi:10.1007/s13738-013-0375-5
99. Subramaniam R, Ponnusamy SK. Novel adsorbent from agricultural waste (cashew nut shell) for methylene blue dye removal: Optimization by response surface methodology. Water Res Indus. 2015;11:64–70. doi:10.1016/j.wri.2015.07.002
100. AlOthman Z, Habila M, Ali R. Preparation of activated carbon using the copyrolysis of agricultural and municipal solid wastes at a low carbonization temperature. Carbon. 2011;24:67–72. doi:10.13140/2.1.1478.2401
101. Kang C, Shang D, Yang T, Zhu L, Liu F, Wang N, Tian T. Preparation of corn stalk-walnut shell mix-based activated carbon and its adsorption of malachite green. Chem Res Chin Univ. 2018;34(6):1014–1019. doi:10.1007/s40242-018-8045-x
102. Haki AM, Imgharn A, Aarab N, Hsini A, Essekri A, Laabd M, El-Jazouli H, Elamine M, Lakhmiri R, Albourine A. Efficient removal of crystal violet dye from aqueous solutions using sodium hydroxide- modified avocado shells: Kinetics and isotherms modeling. Water Sci Technol. 2022;85(1):433–448. doi:10.2166/wst.2021.451
103. Khang DS, Hai TD, Thi TD, Tuan PD. Dye removal using cashew nut shell activated carbon. Viet J Chem. 2020;58(6):832–840. doi:10.1002/vjch.202000096
104. Rocha PD, Franca AS, Oliveira LS. Batch and column studies of phenol adsorption by an activated carbon based on acid treatment of corn cobs. Int J Eng Tech. 2015;7(6):459–464. doi:10.7763/IJET.2015.V7.837
105. Nazari G, Abolghasemi H, Esmaieli M, Assar M. Theoretical and experimental study of cephalex in batch adsorption dynamics using walnut shell-based activated carbon. Des Wat Treat. 2016;57(56):27339–27348. doi:10.1080/19443994.2016.1172029
106. Menkiti MC, Aneke MC, Ejikeme PM, Onukwuli OD, Menkiti NU. Adsorptive treatment of brewery effluent using activated Chrysophyllum albidium seed shell carbon. SpringerPlus. 2014;3(213):1–19. doi:10.1186/2193-1801-3-213
107. Sellaoui L, Yazidi A, Taamalli S, Bonilla-Petriciolet A, Louis F, El Bakali A, Badawi M, Lima EC, Lima DR, Chen Z. Adsorption of 3-aminophenol and resorcinol on avocado seed activated carbon: Mathematical modelling, thermodynamic study and description of adsorbent performance. J Molec Liquids. 2021;342:1–7. doi:10.1016/j.molliq.2021.116952
108. Rahman MM, Adil M, Yusof AM, Kamaruzzaman YB, Ansary RH. Removal of heavy metal ions with acid activated carbons derived from oil palm and coconut shells. Mater. 2014;7(5):3634–3650.
109. Erhayem M, Al-Tohami F, Mohamed R, Ahmida K. Isotherm, kinetic and thermodynamic studies for the sorption of mercury (II) onto activated carbon from Rosmarinus officinalis Leaves. Am J Anal Chem. 2015;6:1-10. doi:10.4236/ajac.2015.61001
110. Maheshwari U, Mathesan B, Gupta S. Efficient adsorbent for simultaneous removal of Cu(II), Zn(II) and Cr(VI): Kinetic, thermodynamics and mass transfer mechanism. Proc Safety Environ Pro. 2015;98:198–210. doi:10.1016/j.psep.2015.07.010
111. Salman T, Aydın TF, Turan G, Ardalı Y. Removal of lead (II) from aqueous solution by batch adsorption on various inexpensive adsorbents using experimental design. Des Wat Treat. 2014;56:1–10. doi:10.1080/19443994.2014.951073
112. El-Naggar AH, Alzhrani AKR, Ahmad M, Usman ARA, Mohan D, Ok YS, Al-Wabel MI. Preparation of activated and non-activated carbon from conocarpus pruning waste as low-cost adsorbent for removal of heavy metal ions from aqueous solution. BioResources. 2016;11(1):1092–1107. doi:10.15376/biores.11.1.1092-1107
113. Mise S, Patil TN. Adsorption studies of chromium(VI) on activated carbon derived from mangifera indica (mango) seed shell. J Inst of Eng (India) Ser A. 2015;96(3):237–247. doi:10.1007/s40030-015-0124-0
114. Siripatana C, Khuenpetch A, Phromrak R, Saengngoen W, Nuithitikul K. Kinetic study of adsorption of lead (II) Ions onto cashew nut shells. ARPN J Eng Appl Sci. 2017;2(7):1819–1824. doi:10.3923/jeasci.2017.1819.1824
115. Nuithitikul K, Phromrak R, Saengngoen W. Utilization of chemically treated cashew-nutshell as potential adsorbent for removal of Pb(II) ions from aqueous solution. Sci Rep. 2020;10(1): 3343–3357. doi:10.1038/s41598-020-60161-9
116. Deokar SK, Mandavgane SA, Kulkarni BD. Adsorptive removal of 2,4-dichlorophenoxyacetic acid from aqueous solution using bagasse fly ash as adsorbent in batch and packed-bed techniques. Clean Tech Environ Pol. 2016;17:1–13. doi:10.1007/s10098-016-1124-0
117. Chatterjee A, Schiewer S. Biosorption of cadmium(II) ions by citrus peels in a packed bed column: Effect of process parameters and comparison of different breakthrough curve models. Clean-Soil Air Water. 2011;239(9):874–881. doi:10.1002/clen.201000482
118. Calero M, Blázquez G, Ronda A, Álvarez AE, Martín-Lara, M. Á. Biosorption of Cu^{2+} in a packed bed column by almond shell : Optimization of process variables. Des Water Treat. 2013;51(2):1954–1964. doi:10.1080/19443994.2012.715167
119. López-Cervantes J, Sánchez-Machado DI, Sánchez-Duarte RG, Correa-Murrieta MA. Study of a fixed-bed column in the adsorption of an azo dye from an aqueous medium using a chitosan–glutaraldehyde biosorbent. Adsorp Sci Technol. 2018;36(1–2):215–232. doi:10.1177/0263617416688021
120. Bohart GS, Adams EQ. Some aspects of the behaviour of the charcoal with respect to chlorine. J Am Chem Soc. 1920;42:523–544. doi:10.1021/ja01448a018
121. Rout PR, Dash RR, Bhunia P. Modelling and packed bed column studies on adsorptive removal of phosphate from aqueous solutions by a mixture of ground burnt patties and red

soil. Adv Environ Res. 2014;3(3):231–251. doi:10.12989/aer.2014.3.3.231
122. Ghribi A, Chlendi M. Modeling of fixed bed adsorption: Application to the adsorption of an organic dye. Asian J Tex. 2011;1(4):161–171. doi:10.3923/ajt.2011.161.171
123. El-Naas MH, Alhaija MA, Al-Zuhair S. Evaluation of an activated carbon packed bed for the adsorption of phenols from petroleum refinery wastewater. Environ Sci PollUT Res. 2017;24(8):7511–7520. doi:10.1007/s11356-017-8469-8
124. Yoon YH, Nelson JN. Application of gas adsorption kinetics I: A theoretical model for respirator cartridge service life. The Amer Indus Hyg Assoc J. 1984;45(8):509–516. doi:10.1080/15298668491400197
125. Kavak, D, Öztürk N. Adsorption of boron from aqueous solution by sepirolite: II. Column studies. II. Illuslrararasi Bor Sempozyumu. 2004;23-25:495–500.
126. Yan G, Viraraghavan T, Chen M. A new model for heavy metal removal in a biosorption column. Ads Sci Technol. 2001;19(1):25–43. doi:10.1260/026361701149395
127. Kumar SR, Vijayaraghavan K, Thilakavathi M, Iyer PVR, Velan M. Seaweeds for the remedition of wastewaters contaminated with zinc (II) ions. J Haz Mater. 2006;136(3):791–799. doi:10.1016/j.jhazmat.2006.01.014
128. Araneda C, Basualto C, Sapag J, Tapia C, Cotoras D, Valenzuela F. Uptake of copper (II) ions from acidic aqueous solutions using a continuous column packed with microcapsules containing a β-hydroxyoximic compound. Chem Eng Res Des. 2011;89(12):2761–2769. doi:10.1016/j.cherd.2011.05.008
129. Khanh NH, Hoang NV. Adsorption process on fixed bed column in rich organic wastewater treatment experimental studies and numerical simulation. Vietnam J Mech. 2006;28(1):28–34. doi:10.15625/0866-7136/28/1/5476
130. Dinesha BL, Hiregoudar S, Nidoni U, Ramappa KT, Dandekar AT, Ganachari SV. Adsorption modelling and fixed-bed column study on milk processing industry wastewater treatment using chitosan zinc-oxide nano- adsorbent–coated sand filter bed. Environ Sci Pollut Res. 2022;30(13):37547–37569. doi:10.1007/s11356-022-24873-x
131. Mavinkattimath RG, Shetty Kodialbail V, Srinikethan, G. Continuous fixed-bed adsorption of reactive azo dye on activated red mud for wastewater treatment-Evaluation of column dynamics and design parameters. Environ Sci Pollut Res. 2023;30(19):57058–57075. doi:10.1007/s11356-023-26210-2
132. Mendes PAP, Rodrigues AE, Almeida JP, Silva JAC. Dynamics of a Fixed Bed Adsorption Column in the Kinetic Separation of Hexane Isomers in MOF ZIF-8. In Pinto AA, Zilberman D. (Eds.), Modeling, Dynamics, Optimization and Bioeconomics III.1st eds. Cham: Springer International Publishing. 2018;224:257–271. doi:10.1007/978-3-319-74086-7_12
133. Anisuzzaman SM, Bono A, Krishnaiah D, Tan YZ. A study on dynamic simulation of phenol adsorption in activated carbon packed bed column. JKing Saud Uni Eng Sci.2014;30:1–30.
134. Arim AL, Neves K, Quina MJ, Gando-Ferreira LM. Experimental and mathematical modelling of Cr(III) sorption in fixed-bed column using modified pine bark. J Cleaner Product. 2018;183:272–281. doi:10.1016/j.jclepro.2018.02.094
135. Haroon H, Shah JA, Khan MS, Alam T, Khan R, Asad SA, Ali MA, Farooq G, Iqbal M, Bilal M. Activated carbon from a specific plant precursor biomass for hazardous Cr(VI) adsorption and recovery studies in batch and column reactors: Isotherm and kinetic modeling. J Water Process Eng. 2020;38:101–577. doi:10.1016/j.jwpe.2020.101577
136. Antil M, Singh S, Bhagat M, Vilvas V, Sundaramurthy S. Column optimization of adsorption and evaluation of bed parameters-based on removal of arsenite ion using rice husk. Environ Sci Pollut Res. 2022:1–15. doi:10.1007/s11356-022-20580-9
137. Warren D, Seider J, Seader JD, Lewin DR. Process Design Principles: Synthesis, Analysis, and Evaluation. New York: John Wiley and Sons; 1999. 766 p.
138. Kalogirou SA, Panteliou S, Dentsoras A. Artificial Neural Networks used for performance prediction of a thermosiphon solar water heater. Renewable Energy. 1999;18(1):87–99. doi:10.1016/S0960-1481(98)00787-3
139. Nascimento CAO, Giudici R, Guardani R. Neural network based approach for optimization of industrial chemical processes. 2000;24:2303–2314. doi:10.1016/S0098-1354(00)00587-1
140. Ayoub MA, Almansour AO, Hassan AM. A novel formula for estimating oil compressibility below bubble point pressure using group method of data handling: A comparative approach. In SPE/IATMI Asia Pacific Oil and Gas Conference and Exhibition. 2019 Oct 29-31; Bali, Indonesia. p. 12. doi:10.2118/196446-MS
141. Stanley FJ. The GMDH Algorithm of Ivakhnenko. Am Stat. 1981;35(4):210–215. doi:10.2307/2683292
142. Madala HR, Ivakhneko OG. Inductive learning algorithms for complex systems modeling. GMDH book. Boca Raton USA: CRC Press. 1994. 373 p.
143. Voss, MS. The Group Method of Cartesian Programming: A New Methodology for Complex Adaptive Functional Networks[dissertation]. Wisconson (USA):Marquette University; 2002. 261 p.
144. Sahu JN, Acharya J, Meikap BC. Optimization of production conditions for activated carbons from tamarind wood by zinc chloride using response surface methodology. Biores Tech. 2010;101(6):1974–1982. doi:10.1016/j.biortech.2009.10.031
145. Betiku E, Osunleke AS, Odude VO, Bamimore A, Oladipo B, Okeleye AA, Ishola NB. Performance Evaluation of Adaptive Neuro-Fuzzy Inference system, Artificial Neural Network and Response Surface Methodology in Modeling Biodiesel Synthesis from Palm Kernel Oil by Transesterification. Biofuels. 2018. doi:10.1080/17597269.2018.1472980.
146. Bhowmik M, Kanmani M, Animesh D, Biswajit S. Sono-assisted rapid adsorption of anionic dye onto magnetic $CaFe_2O_4/MnFe_2O_4$ nanocomposite from aqua matrix. Powder Technol. 2019;354:496–504. doi:10.1016/j.powtec.2019.06.009
147. Razzaq L, Abbas MM, Miran S, Asghar S, Nawaz S, Soudagar MEM, Shaukat N, Veza I, Khalil S, Abdelrahman A. Response surface methodology and artificial neural networks-based yield optimization of biodiesel sourced from mixture of palm and cotton seed oil. Sustainab. 2022;14:6130. doi:10.3390/su14106130
148. Thoai DN, Tongurai C, Prasertsit K, Kumar A. Predictive capability evaluation of RSM and ANN in modeling and optimization of biodiesel production from palm (Elaeisguineensis) oil. Int J Appl Eng Res. 2018;13:7529–7540.
149. Farobie O, Hasanah N, Matsumura Y. Artificial neural network modeling to predict Biodiesel production in supercritical methanol and ethanol using spiral reactor. Proc Environ Sci. 2015;28:214–223. doi:10.1016/j.proenv.2015.07.028
150. Haryanto A, Saputra TW, Telaumbanua M, Gita AC. Application of artificial neural network to predict biodiesel yield from waste frying oil transesterification. Ind J Sci Technol. 2019;5:62–74. doi:10.17509/ijost.v5i1.23099
151. Mahfouz AB, Ali A, Crocker M, Ahmed A, Nasir R, Show PL. Neural-network-inspired correlation (N2IC) model for estimating biodiesel conversion in algal biodiesel units. Fermentation. 2023;9:47. doi:10.3390/fermentation9010047